Tampere University

Claudiu-Eugen Bota

ANALYSIS AND COMPARISON OF CP-OFDM AND UW-OFDM

Electrical Engineering
Master of Science Thesis
October 2019

ABSTRACT

Claudiu-Eugen Bota: Analysis and comparison of CP-OFDM and UW-OFDM
Master of Science Thesis
Tampere University
Wireless Communications and RF Systems
October 2019

Society is in a process of continuous innovation, where the requirements are more and more demanding. Therefore, new mobile network technologies appear with the objective of meeting all these new needs, such as 5G New Radio.

The goal of this thesis is to analyze 5G New Radio in high speed scenarios, implementing it in MATLAB according to 3GPP specifications. Starting with MATLAB's 5G Toolbox, certain modifications are made in order to test all the different scenarios for some chosen velocities. To do this, different values of a series of parameters that affect the throughput are tested. Hence, the throughput is the characteristic used to measure the performance of 5G New Radio in this thesis.

Among these parameters are the subcarrier spacing, the carrier frequency and the number of DMRS reference symbols. Once this is known, different configurations are made, analyzing how they affect the throughput, focusing mostly on two high velocities: 160 km/h and 240 km/h. The results show that increasing the spacing subcarrier and the number of DMRS symbols, increases the throughput also, while it is decreased if either the carrier frequency or the user's speed increases, as the last ones increase the Doppler shift.

Finally, a comparison is made between the waveform proposed by 5G New Radio, CP-OFDM, and an alternative called UW-OFDM. This UW-OFDM brings numerous benefits compared to CP-OFDM, and it is concluded that the throughput it offers is superior to the one CP-OFDM offers in these high speed scenarios.

Keywords: 5G, CP-OFDM, UW-OFDM, subcarrier, throughput

PREFACE

First of all, I want to acknowledge my thanks to my parents. I want to thank you all the effort and sacrifices you had to do to allow me to study a degree at the university. They have been always there to encourage me in the bad moments. They are the persons I most admire for their humility, perseverance and optimism, and I hope I will be like them. I lack words to express my gratitude for everything they have done for me.

Secondly, I want to thank my friends and classmates. Without them I would not be where I am. Thanks for the laughs during exam periods and for the support through all these years.

Finally, I want to thank my tutors Toni Levanen, Jukka Talvitie and Mikko Valkama for the patience they had and for all their help throughout the duration of this work. I can not express my gratitude for all the opportunities they gave to me and for not giving up on me, even though I did sometimes.

Tampereella, 16th October 2019

Claudiu-Eugen Bota

CONTENTS

LIST OF FIGURES

LIST OF TABLES

LIST OF SYMBOLS AND ABBREVIATIONS

$\bar{H_c}$	Diagonal matrix containing the sampled channel frequency response
$\bar{H}$	Diagonal matrix containing the sampled channel frequency response after extracting the zero subcarriers
$\bar{c}$	Codeword of a systematic complex number Reed-Solomon code in frequency domain
$\bar{d}$	Data vector in frequency domain
$\bar{r}$	Vector containing redundant subcarriers in frequency domain
$\bar{x}$	Data vector and zeros subcarriers in frequency domain
$\bar{x}_u$	Unique word vector in frequency domain
$\bar{y}$	Received UW-OFDM symbol in frequency domain after extracting the zero subcarriers and the influence of the unique word
$\bar{y}_d$	Received UW-OFDM symbol in frequency domain after extracting the zero subcarriers
$\Delta f_{Doppler}$	Doppler shift
Δf	Subcarrier spacing
$\check{G}$	Code generation matrix for the non-systematic coding
$\hat{d}$	Estimated data vector in frequency domain
μ	Subcarrier spacing configuration, $\Delta f = 2^{\mu} \cdot 15[kHz]$
σ_d	Standard deviation of the data
σ_n	Standard deviation of the noise
τ_{max}	Maximum delay of a time-varying and multipath fading channel
3GPP	3rd generation partnership project
4G	Fourth generation (mobile communications technologies)
5G	Fifth generation (mobile communications technologies)
A	Non-singular real matrix
A_{opt}	Optimal non-singular real matrix
AWGN	Additive White Gaussian Noise
B	Zero padding matrix
BER	Bit error rate

BW	Bandwidth
$C_{\bar{e}\bar{e}}$	Error covariance matrix
$c_{k,l}$	Subcarrier modulating symbol
CDL	Clustered delay line
CP	Cyclic prefix
CP-OFDM	Cyclic Prefix - Orthogonal Frequency Division Multiplexing
DFT	Discrete Fourier Transform
DL	Downlink
DMRS	Demodulation reference signals
E	Equalizer used in UW-OFDM
E-UTRA	Evolved Universal Terrestrial Radio Access
$E_x^{'}$	Average symbol energy
E_{BLUE}	Best linear unbiased estimator
E_{LMMSE}	Linear minimum mean square error estimator
EDGE	Enhanced Data Rates for GSM of Evolution
eMBB	Enhanced Mobile Broadband
F_N	FFT of size N
F_N^{-1}	IFFT of size N
f_c	Carrier frequency
f_k	Frequency of subcarrier k
f_u	Frequency of subcarrier u
f_v	Frequency of subcarrier v
FDM	Frequency Division Multiplexing
FFT	Fast Fourier Transform
FR_1	Frequency range 1
FR_2	Frequency range 2
G	Code generation matrix
GSM	Global System for Mobile communications
h	Vector of channel impulse response coefficients
H_c	Cyclic convolution matrix obtained from h
HSDPA	High-Speed Downlink Packet Access
I	Identity matrix
ICI	Inter-carrier interference
IDFT	Inverse Discrete Fourier Transform

IFFT	Inverse Fast Fourier Transform
ISI	Inter-symbol interference
J_E	Cost function of the average symbol energy
KSP	Known Symbol Padding
LTE	Long Term Evolution
LTE-A	Long Term Evolution - Advanced
MIMO	Multiple-input multiple-output
MMSE	Minimum mean square error
mMTC	Massive Machine Type Communications
N	Total number of subcarriers
n	Zero-mean Gaussian noise vector
N_d	Size of the data vector in frequency domain
N_r	Size of the redundant subcarriers vector
N_u	Size of the unique vector
N_{frame}^{slot}	Number of frames per slot
N_{RB}	Number of resource blocks
N_{RB}^{μ}	Number of resource blocks per numerology
N_{SC}	Number of subcarriers
N_{SC}^{RB}	Number of subcarriers per resource block
N_{slot}^{frame}	Number of slots per frame
$N_{slot}^{subframe}$	Number of slots per subframe
N_{symb}	Number of symbols
N_{symb}^{μ}	Number of symbols per numerology
N_{symb}^{slot}	Number of symbols per slot
NR	New radio
OFDM	Orthogonal Frequency Division Multiplexing
P	Permutation matrix
P_{avg}	Average power
PAPR	Peak to average power ratio
PDSCH	Physical downlink shared channel
QAM	Quadrature amplitude modulation
R_{symb}	Symbol rate
RB	Resource block
RE	Resource element

RG	Resource grid
RMS	Root-mean-squared
SC-FDMA	Single Carrier Frequency Division Multiplexing Access
SCS	Subcarrier spacing
SISO	Single-input single-output
SNR	Signal-to-noise ratio
T	Period of a periodic signal
t	Continuous time
T_{CP}	Period of the CP
T_{DFT}	Period of the DFT
T_e	Period of the extended symbol
T_{GI}	Period of the guard interval
T_{slot}	Period of the slot
T_{symb}	Period of the symbol
TDM	Time Division Multiplexing
UE	User equipment
UMTS	Universal Mobile Telecommunication System
URLLC	Ultra Reliable Low Latency Communications
UW	Unique word
UW-OFDM	Unique Word - Orthogonal Frequency Division Multiplexing
v	Velocity
W	Data vector affected by the non-singular real matrix
x	UW-OFDM symbol in time domain with unique word 0
$x^{'}$	UW-OFDM symbol in time domain
x_d	Data vector in time domain
x_u	Unique word vector in time domain
y_r	Received UW-OFDM symbol in time domain
ZF	Zero forcing

1 INTRODUCTION

1.1 Background

Society is in a period where needs constantly change, and therefore, new technologies appear in order to satisfy them. In the past, the need of the human being to be able to communicate remotely led to the development of mobile networks. Initially, the main use of these networks was voice communication, and therefore, all technologies such as Global System for Mobile communications (GSM) were based on circuit switching [1],[2].

Subsequently, people demanded a greater use of mobile data, which led to the emergence of technologies such as Universal Mobile Telecommunication System (UMTS) or Enhanced Data rates for GSM of Evolution (EDGE), which added to the classic circuit switching a new way of switching: packet switching [1],[2]. The great usefulness of the data packets led to a change in the direction in which the mobile networks were going to, focusing only on packet switching.

Long Term Evolution (LTE) was the first of the technologies that was completely based on packet switching, and for a long time, together with its successor Long Term Evolution - Advanced (LTE-A), they were able to meet people's needs [2]. However, the great industrial revolution in which we find ourselves requires better performance which the fifth generation (5G) mobile communications technologies seek to satisfy. In order to do so, the standards organization which is in charge of the creation of protocols for mobile telephony, the 3rd generation partnership project (3GPP), has developed the 5G New Radio (5G NR) radio access technology [1].

This new technology is designed to be very flexible, adapt to different scenarios and have many applications. One of those applications relates to high speed devices, whose importance seems to not stop increasing, as they are used in both military and civil fields. From trains to drones and planes, high speed devices have gained a big importance in today's society.

1.2 Objectives

The main objective of this thesis is to analyze the performance of 5G NR with high speed devices, using the MATLAB 9.7 5G Toolbox. However, this 5G Toolbox is not complete as it does not work for higher velocities, so all those functionalities not provided are imple-

mented in such a way that respects the 3GPP specifications. In order to do so, numerous tests are going to be carried out, analyzing the effect of all the influential parameters on the throughput, which will be the characteristic that is measured to analyze the performance of 5G NR.

The main idea is to find those configurations that maximize transmission speed for high speed scenarios, and analyze how it decays based on certain parameters. In this thesis, the effect of following parameters is analyzed: subcarrier spacing, carrier frequency, and number of Demodulation Reference Signals (DMRS) symbols. For a set of high velocities, different configurations of these parameters will be tested, analyzing how they influence the throughput and which of these parameters are the most relevant in these high speed scenarios.

In addition, a comparison will be made between the waveform established by the 3GPP specifications for 5G NR, Cyclic Prefix - Orthogonal Frequency Division Multiplexing (CP-OFDM), with an alternative waveform proposed by some experts called Unique Word - Orthogonal Frequency Division Multiplexing (UW-OFDM) [3],[4],[5]. This alternative seems to offer lower error rates in high speed scenarios, and therefore, higher throughput. A comparison will be made in terms of throughput, analyzing the pros and cons of UW-OFDM, to determine whether or not it is a viable alternative to the classic CP-OFDM in the mentioned high speed scenarios.

2 INTRODUCTION TO 4G AND 5G MOBILE COMMUNICATIONS TECHNOLOGIES

2.1 4G mobile communications technologies (LTE and LTE-A)

2.1.1 Introduction

The constant increase in the number of mobile network users, made telecommunications companies look for new alternatives in order to fulfill these new needs that previous communications technologies such as UMTS or High-Speed Downlink Packet Access (HSDPA) could not. These technologies do not meet the capacity, speed and latency requirements of the emerging trends, and the emergence of applications increasingly dependent on mobile data only accelerated the development of more appropriate alternatives.

Based on these requirements, LTE arises as a technology that seeks to meet the requirements of the standards of fourth generation or 4G mobile networks. The main requirements of 4G are: physical layer latency in connected mode of 10 ms; peak data rates of 1 Gbps; 20 MHz channel bandwidth; CP-OFDM as the waveform for the downlink channel; and Single Carrier Frequency Division Multiplexing Access (SC-FDMA) as the waveform for uplink channel [6],[7].

LTE, however, fails to meet the higher current requirements but establishes the waveform which future generations of mobile networks will be developed on: CP-OFDM.

2.1.2 Frame structure in LTE

Time is divided in N_{symb} OFDM symbols and the frequency is divided in $N_{RB} * N_{SC}$ subcarriers. Each pair of subcarrier-OFDM symbol represents a unique division which is called Resource element (RE), which can form a larger entity called Resource block (RB) [8]. In turn, these RBs form the Resource grid (RG), which represents all the resources which have been divided in the REs as it can be seen in figure 2.1:

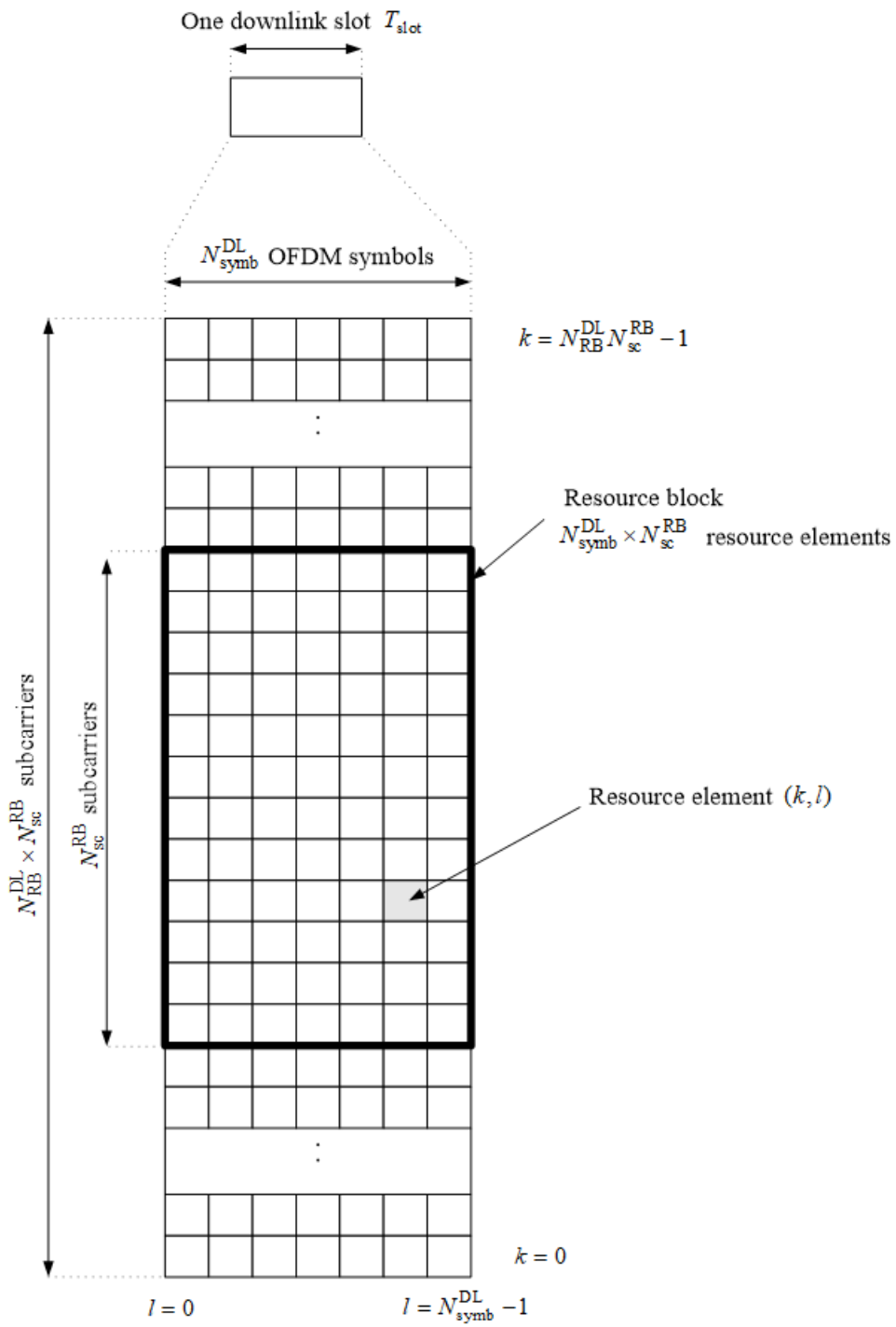

Figure 2.1. *Downlink resource grid in CP-OFDM for LTE*
Figure 6.2.2-1 [7]

As it can be seen in the figure 2.1, each resource grid has a duration of a T_{slot} timeslot. Therefore, each slot can contain N_{RB} RBs. In addition, the frame has a duration of 10 ms and is formed in turn by 10 subframes of 1 ms each. These subframes, in turn, are formed by two slots that are the ones that contain the RBs as mentioned before. Therefore, the duration of these slots, and therefore the duration of the OFDM symbols that are part of the RB, is 0.5 ms.

These RBs, in addition to having a duration of one timeslot, also occupy 180 kHz in frequency. The REs represent an OFDM symbol on a subcarrier, while an RB represents 7 or 6 OFDM symbols, depending on whether there is normal or extended cyclic prefix, over 12 subcarriers [8]. This can be seen in the table 2.1, which also includes the spacing between the different subcarriers.

Table 2.1. *Physical resource block parameters*

Table 6.2.3-1 [8]

Configuration		N_{sc}^{RB}	N_{symb}^{DL}
Normal cyclic prefix	$\Delta f = 15\,\text{kHz}$	12	7
Extended cyclic prefix	$\Delta f = 15\,\text{kHz}$		6
	$\Delta f = 7.5\,\text{kHz}$	24	3
	$\Delta f = 1.25\,\text{kHz}$	144	1

From the table 2.2 and as mentioned above, it can be understood that the resource grid will consist of a certain number of RBs, which have the dimensions mentioned. This number varies between 6 and 100 RBs, depending on the bandwidth chosen from among all possible values between 1.4 and 20 MHz [8].

Table 2.2. *Transmission bandwidth configuration N_{RB} in Evolved Universal Terrestrial Radio Access (E-UTRA) channel bandwidths*

Table 5.6-1 [8]

Channel bandwidth $BW_{Channel}$ [MHz]	**1.4**	**3**	**5**	**10**	**15**	**20**
Transmission bandwidth configuration N_{RB}	6	15	25	50	75	100

2.2 5G mobile communications technologies

2.2.1 Introduction

LTE and its successor, LTE-Advanced, fall short of the challenges that arise as time goes by. The society demands high-speed services, with low latency for critical situations (autonomous vehicles, critical information, etc.), with great capacity to give coverage to all the users of large cities and great scalability to be able to adapt to different situations. To solve these problems, 3GPP has decided to develop what is the new generation of mobile networks: 5G New Radio. The 5G NR requirements can be collected in three

large application areas [9].

First, there is what is called Enhanced Mobile Broadband (eMBB). This application area requires low latency while having also a large throughput, offering a large coverage area. Then, there is Ultra Reliable Low Latency Communications (URLLC). In this case , there are use cases where low latency and high reliability are critical, such as autonomous vehicles or remote surgery. Finally, there is the Massive Machine Type Communications (mMTC). This application area focuses on connecting numerous devices in a small area, so it requires low battery consumption, low device complexity and an improved link budget among others. [9]

2.2.2 Differences with 4G

Despite being based on the same waveform (CP-OFDM) as in 4G, 5G NR presents certain differences and improvements to meet all the requirements mentioned in the previous section. The first of the changes is the introduction of multiple different subcarrier spacings, denoted also as numerologies. While in LTE this was always 15 kHz, in 5G NR there are several more possibilities. Also, 5G NR presents another novelty that is the inclusion of a new frequency range that operates in the millimeter wave (mmWave) frequency range, as well as a variable channel bandwidth of up to 400 MHz which is considerably wider than the 20 MHz supported by LTE [10],[11].

There are other differences and innovations that 5G NR provides with respect to 4G, such as beam management or the deepening of the use of Massive Multiple-input Multiple-output (MIMO), but those mentioned in the previous paragraph are the ones that are going to be analyzed since they have more impact on the physical layer, which is the one that is analyzed in more detail in this thesis.

2.2.3 Frequency range in 5G NR

As mentioned in the previous section, 5G NR operates on two different frequency ranges called FR_1 and FR_2. [10] The range in which these can be found is given in the following table:

Table 2.3. *Definition of frequency ranges for 5G NR*

Table 5.1-1 [10]

Frequency range designation	Corresponding frequency range
FR1	450 MHz – 6000 MHz
FR2	24250 MHz – 52600 MHz

While FR_1 operates in frequency ranges similar to those of LTE with which it shares

spectrum, FR_2 is in much higher frequency ranges to allow high-speed data transmission, but with a lower coverage.

2.2.4 Frame structure in 5G NR

In previous sections, some of the innovations that 5G NR brings about LTE were discussed. Among them, the so-called numerology was mentioned, which is defined by the subcarrier spacing [11]. The different numerologies supported in 5G NR are listed in the following table:

Table 2.4. *Supported transmission numerologies for 5G NR*

Table 4.2-1 [11]

μ	$\Delta f = 2^{\mu} \cdot 15\,[\mathrm{kHz}]$	**Cyclic prefix**
0	15	Normal
1	30	Normal
2	60	Normal, Extended
3	120	Normal
4	240	Normal

Each numerology is therefore assigned a μ index, which is different for all of them, and therefore, determines the distance that separates two subcarriers using the equation in column 2 of table 2.4. It should be noted that 60 kHz is the numerology that can carry both extended and normal CP, which does not occur in the other subcarriers spacings.

The duration of a frame in 5G NR is the same as in LTE, that is, 10 ms, and as in LTE, the frame is made up of 10 subframes of 1 ms each [11]. So far 5G NR behaves the same as LTE, but the influence of numerology is seen when analyzing the slots that make up each subframe.

Table 2.5. *Number of OFDM symbols per slot, slots per frame, and slots per subframe for normal cyclic prefix*

Table 4.3.2-1 [11]

μ	$N^{\text{slot}}_{\text{symb}}$	$N^{\text{frame},\mu}_{\text{slot}}$	$N^{\text{subframe},\mu}_{\text{slot}}$
0	14	10	1
1	14	20	2
2	14	40	4
3	14	80	8
4	14	160	16

As can be seen in the table above, the number of slots depends on numerology, in-

creasing the number of slots per subframe as the spacing subcarrier increases. Also, as numerology increases, the duration of the OFDM symbols decrease while having a fixed sampling rate. This causes shorter slots, and therefore, there are more slots per subframe [11]. As for the extended cyclic prefix, as there is only one numerology used, the number of slots is fixed as shown in the following table:

Table 2.6. *Number of OFDM symbols per slot, slots per frame, and slots per subframe for extended cyclic prefix*

Table 4.3.2-2 [11]

μ	$N_{\text{symb}}^{\text{slot}}$	$N_{\text{slot}}^{\text{frame},\mu}$	$N_{\text{slot}}^{\text{subframe},\mu}$
2	12	40	4

2.2.5 Bandwidth in 5G NR

In 5G NR the maximum transmission bandwidth has the same form as in LTE, that is, N_{RB} RBs. As can be seen in the table below, in addition to dividing the bandwidth between the different RBs, guard bands are needed. When using two different carrier frequencies, the bandwidth and the maximum number of RB therefore varies. For the FR_1 frequency, these data are collected in the following table:

Table 2.7. *Maximum transmission bandwidth configuration N_{RB}*

Table 5.3.2-1 [10]

SCS (kHz)	5MHz	10MHz	15MHz	20 MHz	25 MHz	30 MHz	40 MHz	50MHz	60 MHz	80 MHz	90 MHz	100 MHz
	N_{RB}	N_{RB}	N_{RB}	N_{RB}	N_{RB}	N_{RB}	N_{RB}	N_{RB}	N_{RB}	N_{RB}	N_{RB}	N_{RB}
15	25	52	79	106	133	160	216	270	N/A	N/A	N/A	N/A
30	11	24	38	51	65	78	106	133	162	217	245	273
60	N/A	11	18	24	31	38	51	65	79	107	121	135

Similarly, minimum guard intervals vary with the spacing subcarriers as shown in the following table:

Table 2.8. *Minimum guardband for each User Equipment (UE) channel bandwidth and subcarrier spacing (SCS) (kHz)*

Table 5.3.3-1 [10]

SCS (kHz)	5 MHz	10 MHz	15 MHz	20 MHz	25 MHz	30 MHz	40 MHz	50MHz	60 MHz	80 MHz	90 MHz	100 MHz
15	242.5	312.5	382.5	452.5	522.5	592.5	552.5	692.5	N/A	N/A	N/A	N/A
30	505	665	645	805	785	945	905	1045	825	925	885	845
60	N/A	1010	990	1330	1310	1290	1610	1570	1530	1450	1410	1370

Also, for FR_2 the maximum bandwidth and number of RBs are shown in the table 2.9. Finally, the minimum guard intervals for FR_2 are shown in the table 2.10.

Table 2.9. *Maximum transmission bandwidth configuration N_{RB} for FR2*

Table 5.3.2-2 [12]

SCS (kHz)	50 MHz	100 MHz	200 MHz	400 MHz
	N_{RB}	N_{RB}	N_{RB}	N_{RB}
60	66	132	264	N.A
120	32	66	132	264

Table 2.10. *Minimum guardband for each UE channel bandwidth and SCS (kHz) for FR2*

Table 5.3.3-2 [12]

SCS (kHz)	50 MHz	100 MHz	200 MHz	400 MHz
60	1210	2450	4930	N. A
120	1900	2420	4900	9860

2.2.6 Resource grid

The resource grid is based on the same idea as in the case of LTE. Resources are divided both in time and frequency in the same way, but the main variation is the influence of numerology. As we have seen, as the spacing subcarriers increase, the number of RBs is reduced, and therefore, the resource grid decreases in frequency. On the other hand, the number of slots within a subframe increases, and therefore, there are more OFDM symbols, expanding the resource grid in time. This can best be seen in the following figure:

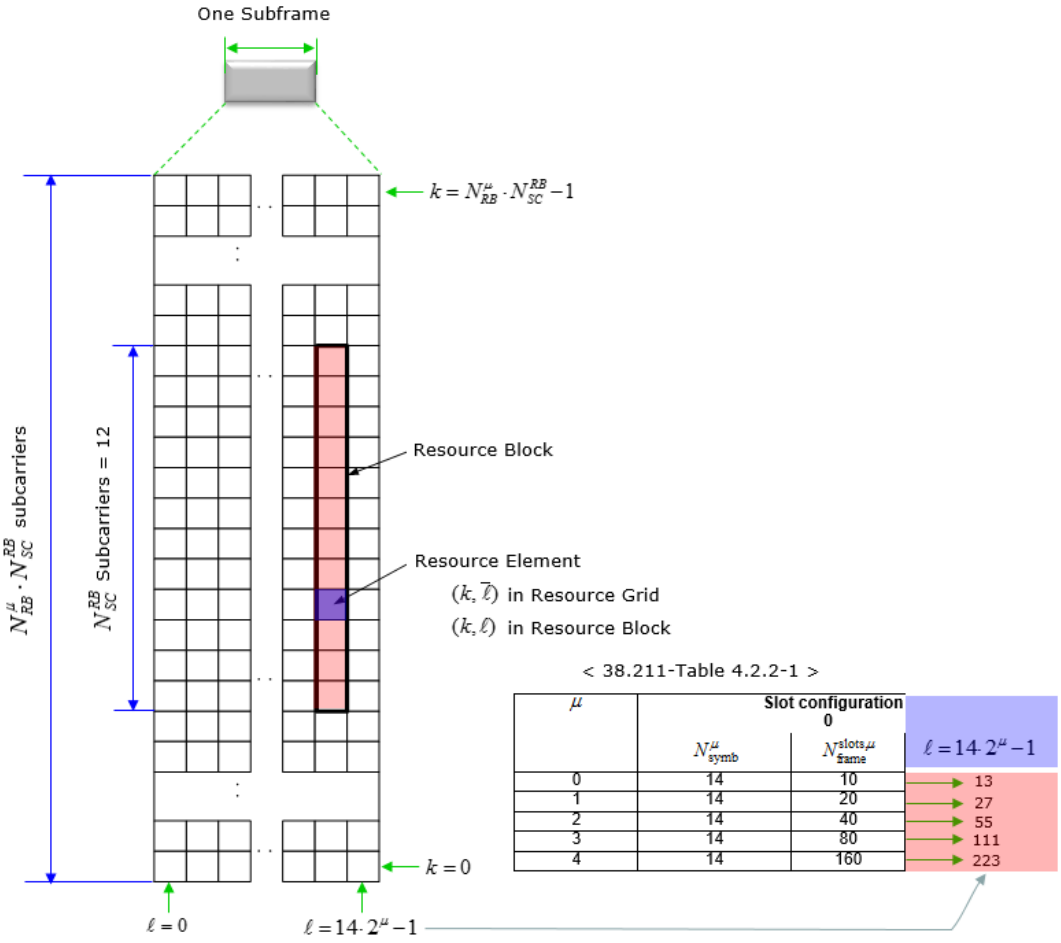

< 38.211-Table 4.2.2-1 >

μ	Slot configuration 0		$\ell = 14 \cdot 2^{\mu} - 1$
	N^{μ}_{symb}	$N^{slots,\mu}_{frame}$	
0	14	10	13
1	14	20	27
2	14	40	55
3	14	80	111
4	14	160	223

Figure 2.2. *Resource grid in 5G*
Resource grid in 5G [13]

2.2.7 Physical downlink shared channel

Among all the physical channels of the downlink, the most relevant in this thesis is the Physical Downlink Shared Channel (PDSCH) and has the same function as in LTE. To understand it better, a high level description of it will be given following [14]:

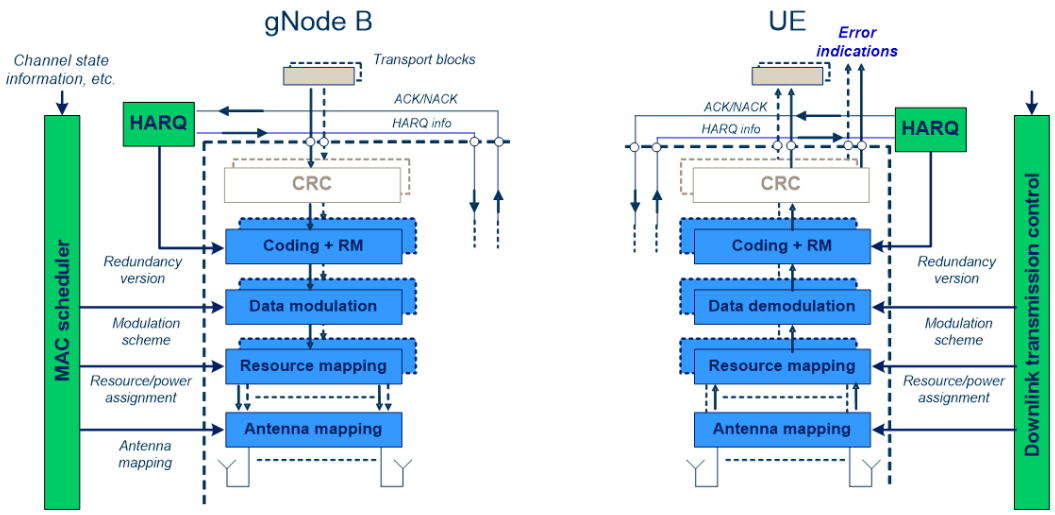

Figure 2.3. *Physical-layer model for DL-SCH transmission*
Figure 5.1.1-1 [14]

The most relevant steps for this PDSCH are the ones contained in the blue boxes in figure 2.3. These steps will only be mentioned, as higher details about them are out of the scope of this thesis but are explained more in detail in [14]. The steps followed by the PDSCH in order to process the data are:

- Higher-layer data passed to/from the physical layer;
- CRC and transport-block-error indication;
- FEC and rate matching;
- Data modulation;
- Mapping to physical resource;
- Multi-antenna processing;
- Support of L1 control and Hybrid-ARQ-related signalling.

2.2.8 Demodulation reference signals for PDSCH

In 5G NR there are numerous important signals, such as synchronization signals [10]. These signals, however, are not going to be analyzed in this thesis, since for the experiments it is assumed that the synchronization is perfect. However, there are other signals that are taken into account, such as DMRS [11].

This signal carries a series of known reference symbols that act similarly to pilots in LTE, known as DMRS symbols. They are important because they are needed for a correct channel estimation. When the transmitted signal is generated, the DMRS symbols are introduced in certain positions depending on different configurations [11]. The DMRS symbols can be placed in different OFDM symbols, as well as in different subcarriers.

When the received signal arrives, the positions where the DMRS were introduced are known. Therefore, from the received signal and the DMRS symbols, it can be established a relationship which helps to estimate the channel. There are different criteria that can be used, such as Zero forcing (ZF) or Minimum mean square error (MMSE). Once the channel is estimated in the positions of the DMRS, a interpolation is done in order to extend this estimation to the whole time-domain resources [11].

As mentioned before, there are different configurations for the DMRS symbols, based on different parameters. The effect of some of these parameters are going to be shown in the following figures, but more details about them can be found in [11].

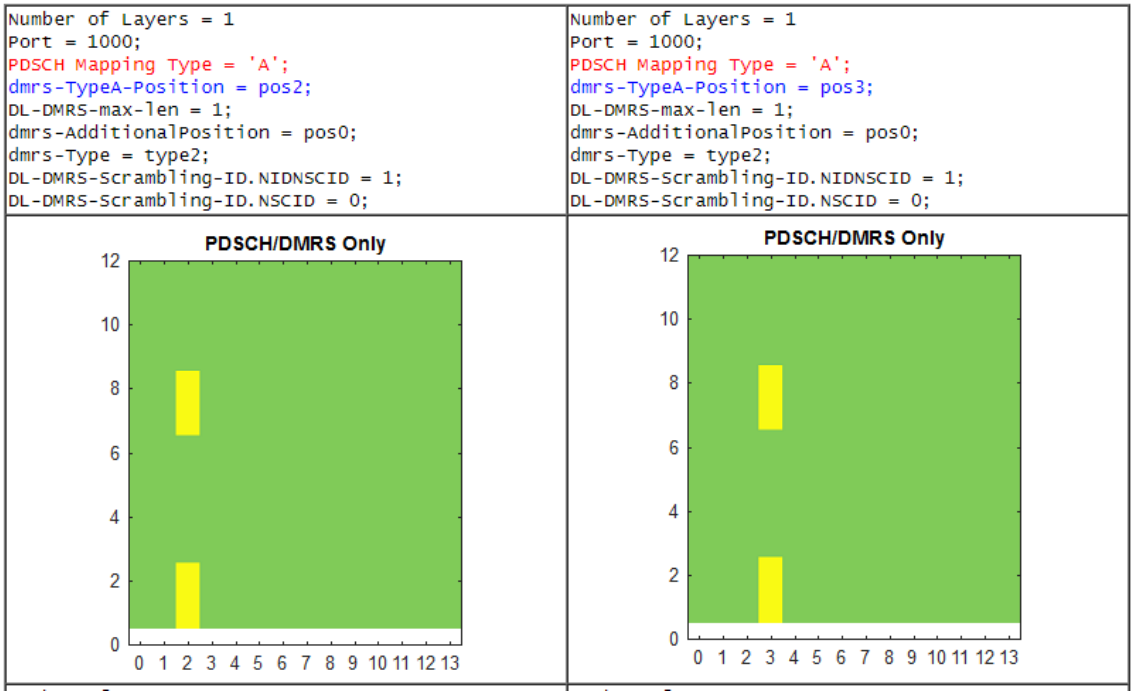

Figure 2.4. *DMRS symbols configuration: first DMRS symbol position*
DMRS symbols configuration [15]

One of the parameters that can be configured when defining the DMRS symbols, is the position of the first DMRS symbol. It can be placed either at the second or the third CP-OFDM symbol as shown in the previous figure.

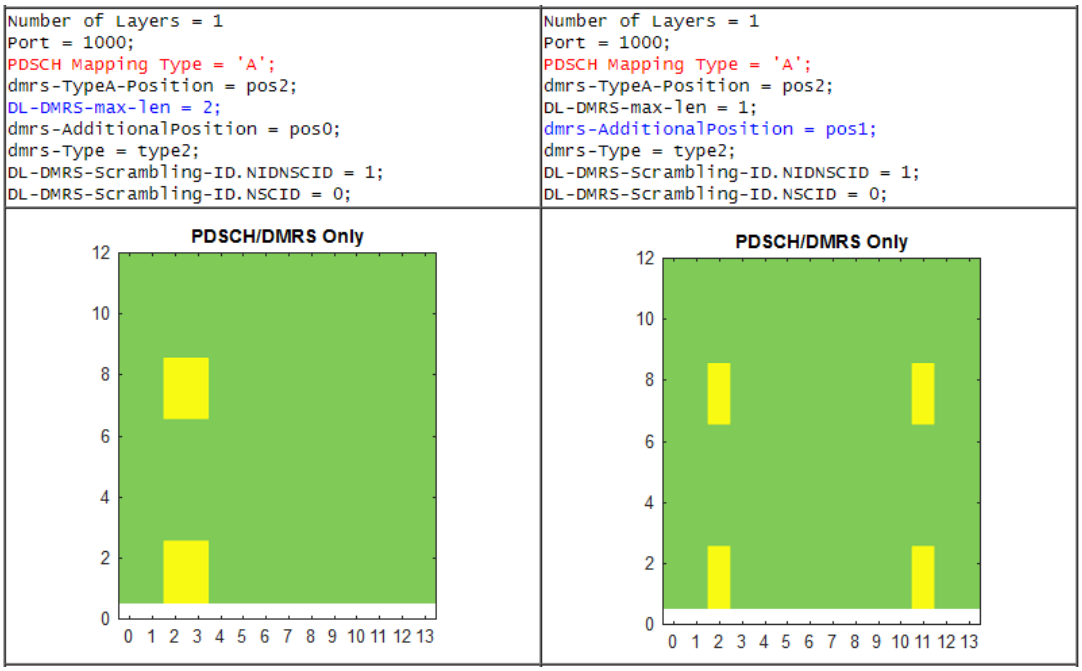

Figure 2.5. *DMRS symbols configuration: single and double symbols*
DMRS symbols configuration [15]

Another option that the DMRS symbols configuration gives, is the possibility of using double DMRS symbols instead of single symbols. Therefore, the DMRS symbol could last two or one CP-OFDM symbol as shown in the figure.

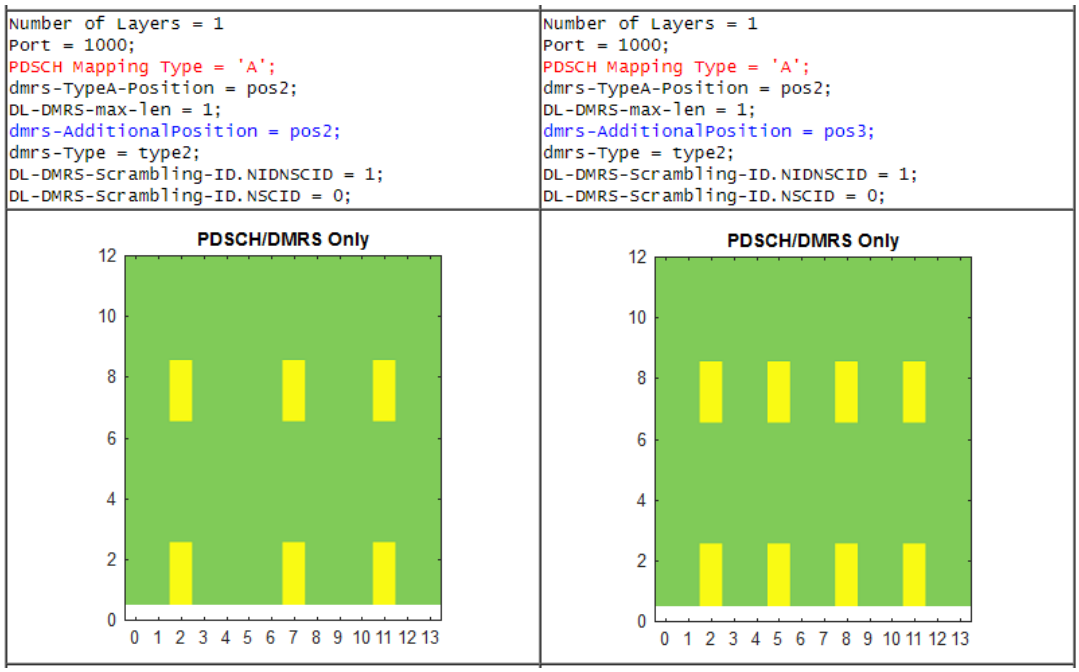

Figure 2.6. *DMRS symbols configuration: additional DMRS symbols*
DMRS symbols configuration [15]

Finally, the last parameter analyzed is the additional DMRS symbols. Initially, there is only 1 DMRS symbol used, but there can be added 3 more DMRS symbols. As it is shown in the previous figure, the DMRS symbol positions change, as there are more DMRS symbols used. These are not the only parameters that can be configured, but are the only ones analyzed in this section [11].

Also, is important to mention that these DMRS symbols are introduced in such a way that, for MIMO scenarios, it is possible to mitigate the interference coming from other paths. For example, when using two layers for mapping the symbols, in the second layer the DMRS symbols are introduced in such a way that it is possible to estimate the different channel's coefficients for each pair of transmitting - receiving antennas. For further details, see [11].

3 THEORETICAL BACKGROUND

3.1 CP-OFDM

3.1.1 Introduction

As it has been discussed in the previous section, CP-OFDM is the waveform recommended by 3GPP in both its 4G and 5G standards [12],[16]. This waveform is being implemented by different telecommunications companies in the deployments of their own 5G networks.

3.1.2 Theoretical background

CP-OFDM is a waveform that is based on the principles of Frequency Division Multiplexing (FDM) [17]. This multiplexing technique consists in dividing the bandwidth between the different users, assigning each one a certain frequency band. The main innovation or difference between CP-OFDM and FDM is the concept of orthogonality that will be analyzed later.

In addition, CP-OFDM is also based on Time Division Multiplexing (TDM) [17], which is a technique that allows several users to use the same bandwidth after dividing it into time units called slots that are assigned to each of them. Therefore, CP-OFDM can be understood as a waveform that combines the benefits of FDM and TDM, and therefore, it divides resources both into slots and subcarriers that are assigned to the different users.

3.1.3 Orthogonality

As mentioned above, CP-OFDM includes the concept of orthogonality as one of the novelties regarding its predecessor, FDM. Unlike the latter, in CP-OFDM the subcarriers which the bandwidth is divided into are orthogonal to each other [18],[19].

As it has been discussed previously, a RB represents the minimum division in which the data is transmitted in 4G or 5G systems, since the REs are not transmitted separately. Therefore, in each transmission of an RB, N_{symb} are sent every T_{slot} seconds as it can be seen in figure 2.1. From here it can be extracted that the period of an CP-OFDM symbol,

with varying CP-length within a subframe is:

$$T_{symb} = \frac{T_{slot}}{N_{symb}} \tag{3.1}$$

And in turn, the symbol rate is:

$$R_{symb} = \frac{1}{T_{symb}} = \frac{N_{symb}}{T_{slot}} \tag{3.2}$$

By using subcarrier orthogonality, the need to use guard bands to separate the subcarriers is eliminated, since the different subbands are hardly affected by their neighbors' emissions. In this way, the spectral efficiency is increased, and what is more, it allows the reduction of the complexity of the receiver by using a fast discrete signal processing which will be analyzed later [17],[18],[19]. Moreover, there is no need to use separate filters for each subcarrier as in FDM [2].

In order to understand the subcarrier wise orthogonality more deeply, we will assume two subcarriers $\Phi_u(t)$ and $\Phi_v(t)$ that have the form:

$$\Phi_u(t) = \frac{1}{\sqrt{T}} e^{2\pi f_u t} \tag{3.3}$$

$$\Phi_v(t) = \frac{1}{\sqrt{T}} e^{2\pi f_v t} \tag{3.4}$$

Where f_u and f_v represent the subcarriers frequencies. To meet the CP-OFDM requirements, these two subcarriers must be orthogonal to each other, and this is only true if they fulfill the following condition:

$$\int_{-\infty}^{+\infty} \Phi_u(t)\Phi_v(t)^* dt = 0 \tag{3.5}$$

$$\frac{1}{T}\int_{0}^{T} e^{2\pi(u-v)\frac{t}{T}} dt = 0 \tag{3.6}$$

Where $\frac{u}{T}$ and $\frac{v}{T}$ represent f_u and f_v respectively. Therefore, the only case in which the orthogonality condition would not be met would be the case in which u and v are equal. As it can be seen in equation 3.6, the minimum distance between the two subcarriers is $u - v = 1$. This means there is a spacing subcarrier such that:

$$\Delta_f = \frac{u-v}{T} = \frac{1}{T} \tag{3.7}$$

One of the main problems of CP-OFDM is the Inter-symbol Interference (ISI). In order to reduce its effects, pulse shaping filters, and more specifically, raised cosine root filters

are applied [20]. With this in mind and applying the filter, the equation of each subcarrier can be defined as follows:

$$\Phi_k(t) = \frac{1}{\sqrt{T}} rect(\frac{t - \frac{T}{2}}{T}) e^{2\pi \Delta f_k t} \tag{3.8}$$

With k = 0,1,2 ..., N-1 and where N is the maximum number of subcarriers.

3.1.4 System in continuous time

In the previous sections it has been explained which is the shape of the subcarriers and how is the frame structure. As it has been shown, N symbols are transmitted every T period [18]. If both concepts are combined, it is obtained that the $l-th$ transmitted OFDM signal has the form:

$$x_l(t) = \sum_{k=0}^{N-1} c_{k,l} \Phi_k(t - lT) \tag{3.9}$$

Where $c_{k,l}$ is the $k-th$ OFDM symbol of the $k-th$ subcarrier of the $l-th$ transmitted OFDM signal, also known as the subcarrier modulating symbol. If a continuous transmission is assumed, then equation 3.9 would be expressed as follows:

$$x(t) = \sum_{l=-\infty}^{+\infty} \sum_{k=0}^{N-1} c_{k,l} \Phi_k(t - lT) \tag{3.10}$$

The OFDM signal is transmitted but is affected by the multipath effect [19],[21]. The signal is transmitted and it arrives following different paths to the receiver, as it is affected by different obstacles. Therefore, all the signals with their respective delays, arrive sumed at the receiver. The channels that present this type of effect are, therefore, time-varying and multipath fading channels and their impulse response is denoted as $h(t, \tau)$.

The channel is not the only thing that affects the transmitted signal, since the Additive White Gaussian Noise (AWGN) expressed as n must be also taken into account. With both ideas in mind, the received signal can be expressed as:

$$r(t) = h(t, \tau) * x(t) + n(t) = \int_0^{\tau_{max}} h(\tau) x(t - \tau) d\tau + n(t) \tag{3.11}$$

Where τ_{max} represents the maximum delay of the channel. It should be noted that a static channel has beed assumed during the transmission of the $k-th$ OFDM symbol, simplifying $h(t, \tau)$ to $h(t)$.

3.1.5 Cyclic prefix

One of the effects of the aforementioned multipath effect is ISI. That is, one among all the received signals, is affected by all the other signals that have taken a different path, thus affecting the symbols received. In order to compensate this, it is necessary to introduce guard bands longer than τ_{max}. This is, to assure there is no overlapping between two received signals [1],[16]. Therefore, it is necessary to introduce what is known as Cyclic Prefix (CP) [18],[19].

The CP is formed by the last samples of a CP-OFDM signal, which are copied and added at the beginning of the mentioned signal, within the guard interval. By doing this, at the receiver it is possible to recover the transmitted signal in a less complex way after eliminating the CP [19]. After knowing this and returning to the equation 3.8, it is obtained that the transmitted signal is defined as:

$$\Theta_k(t) = \frac{1}{\sqrt{T}} rect(\frac{t - \frac{T_e}{2}}{T_e}) e^{2\pi \Delta f_k (t - T_{CP})} \tag{3.12}$$

With k = 0,1,2 ..., N-1 and where $Te = T + T_{CP}$ that makes up the total period of the transmitted signal, once the CP has been added.

3.1.6 System in discrete time

As mentioned previously, one of the objectives of CP-OFDM is to reduce the complexity of the entire system, both the transmitter and the receiver. Since continuous time operations are very complicated, an discrete time implementation of this waveform is chosen. For this, both Fast Fourier Transform (FFT) and Inverse Fast Fourier Transform (IFFT) are used, which are the fast versions of Discrete Fourier Transform (DFT) and Inverse Discrete Fourier Transform (IDFT) [18],[19].

These last two have the form:

$$DFTx[n] = X[i] = \frac{1}{\sqrt{N}} \sum_{n=0}^{N-1} x[n] e^{-j2\pi \frac{1}{N} in} \tag{3.13}$$

$$IDFTX[i] = x[n] = \frac{1}{\sqrt{N}} \sum_{i=0}^{N-1} X[i] e^{j2\pi \frac{1}{N} in} \tag{3.14}$$

With n = 0,1,2 ..., N-1 and i = 0,1,2 ..., N-1. Where $x[n]$ is the discrete sequence on which said DFT and IDFT are applied. With this in mind, and using the equations 3.1 and 3.2, it is obtained that $T_{symb} = T_s/N$ and $f_s = N/T_s$. From this, the sampled version of the

$l-th$ signal transmitted is obtained as:

$$x_l(nT_s) = \frac{1}{\sqrt{N}} \sum_{k=0}^{N-1} c_{k,l} e^{j2\pi \Delta f k n T_s - lT} = \frac{1}{\sqrt{N}} \sum_{k=0}^{N-1} c_{k,l} e^{j2\pi \frac{1}{T} k n T_s} = \frac{1}{\sqrt{N}} \sum_{k=0}^{N-1} c_{k,l} e^{j2\pi \frac{1}{N} k n} \tag{3.15}$$

As it can be seen, this equation corresponds to the IDFT of the signal $x(nT_s)$. Therefore, it is obvious to think that at the receiver, it will be necessary to apply the DFT on the received signal. In order to make use of its fast versions, FFT and IFFT, it is necessary to choose a size N that is a power of 2 [19]. Knowing this, we can finally describe the complete CP-OFDM system in discrete time with the figure 3.1:

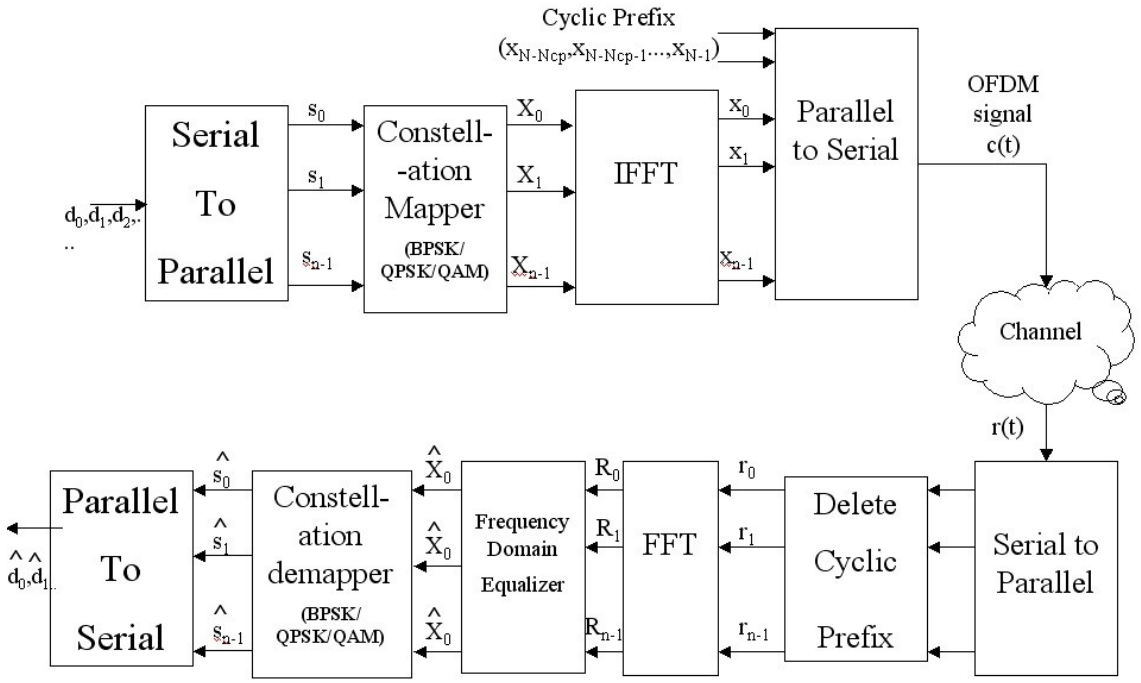

Figure 3.1. *CP-OFDM discrete time system*
Ilustracion 10 [18]

3.1.7 Disadvantages of CP-OFDM

So far we have seen the different advantages that CP-OFDM provides [8],[17],[18], such as the improvement of spectral efficiency or the reduction of the impact ISI by using guard intervals and pilot symbols among others. However, it also has some downsides. One of them is the Peak to Average Power Ratio (PAPR):

$$PAPR = \frac{max|x(t)|^2}{P_{avg}} \tag{3.16}$$

In the case of CP-OFDM, having more subcarriers will deal to a higher numerator and therefore, the PAPR will be also higher.

Another disadvantage of CP-OFDM is its subcarrier frequency synchronization errors [17],[18]. This is due to the difference between the frequencies of the subcarriers in transmitter and receiver, which Inter-carrier Interference (ICI) introduces into the system. Since there is a frequency offset, the subcarrier frequencies are displaced, causing the loss of orthogonality, and therefore, in the receiver it is necessary to compensate it with different techniques.

One of the most widespread techniques is based on the use of pilots. These pilots are a series of transmitted symbols that are previously known and help in the channel estimation [8],[19]. There are different ways of doing this by inserting these pilots either in certain subcarriers, in certain OFDM symbols or in both.

Using the pilots, an interpolation is performed, obtaining a channel estimation, followed by an equalization. Some of the most common methods are ZF and MMSE [18],[19].

3.2 UW-OFDM

3.2.1 Introduction

Despite the total acceptance of CP-OFDM and its various advantages, there are other alternative waveforms that are being studied by experts and, a priori, could solve some of the disadvantages of CP-OFDM while adding numerous other benefits [3],[4],[5].

One of these alternatives is UW-OFDM. UW-OFDM is postulated as a waveform that, according to various studies [3],[4],[5], provides the same results in terms of Bit Error Rate (BER) and throughput than CP-OFDM, if not even better, while reducing the complexity of the system to ensure proper synchronization and estimation of the transmitted data. But to understand this, it is needed to analyze in depth the essence of UW-OFDM.

3.2.2 Comparison with CP-OFDM

This waveform differs from CP-OFDM, mainly in its use of guard intervals [4]. On the one hand, as it has been shown, the guard bands in CP-OFDM are based on the transmitted data and are therefore random. On the other hand, the guard intervals of UW-OFDM are deterministic. This is because these intervals are formed by previously known sequences called unique words.[4]

Similar to UW-OFDM, there is the Known Symbol Padding - OFDM (KSP-OFDM), which also uses deterministic guard intervals known as known symbol [3].The main difference between both of them, is that in UW-OFDM, the UW is part of the DFT, whereas the KS is not. However, KSP-OFDM is out of the scope of this thesis, and it will only be shown in the figure 3.2 to compare its structure with CP-OFDM's and UW-OFDM's.

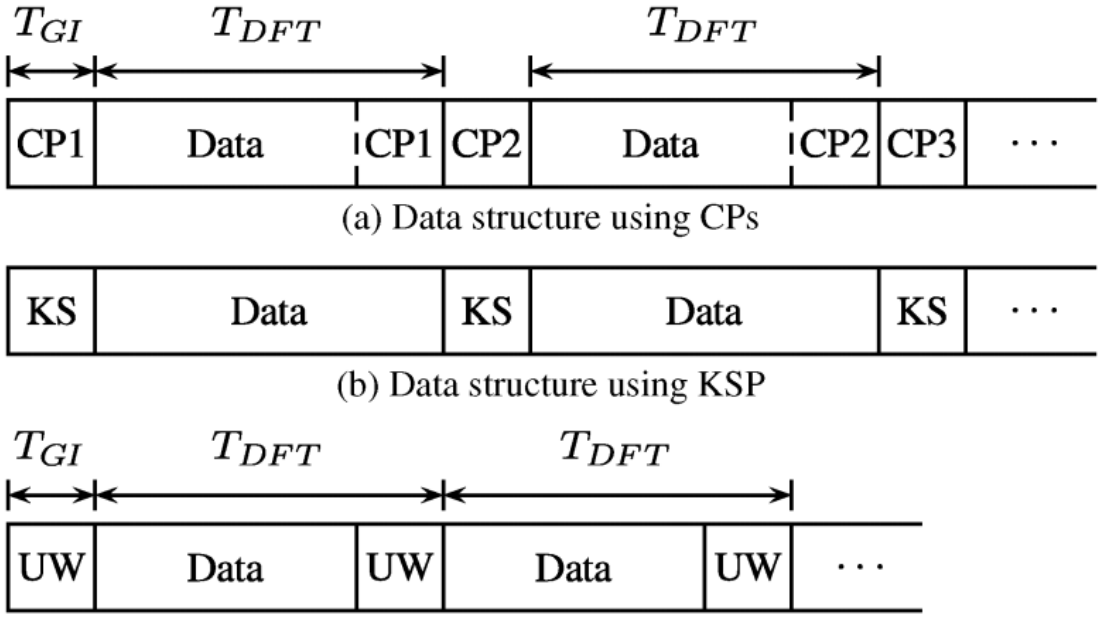

Figure 3.2. *Comparison of the frames in CP-OFDM and UW-OFDM in time domain*
Fig. 1 [3]

The unique words have double functionality: on the one hand, they are used as guard intervals to reduce ISI; and on the other hand, they help in the synchronization and channel estimation.

The latter is achieved through the introduction of redundant subcarriers that introduce a correlation between the different subcarriers, which in turn helps to improve the BER performance [3],[4],[5]. These redundant subcarriers are generated from the data symbols and the permutation matrix, and help to obtain the zero UW needed in the first step of the generation of the UW-OFDM symbol [3],[4],[5]. By doing so, the chosen UW can be added to the UW-OFDM symbol, and latter, it can be extracted at the receiver without affecting the subcarriers in the frequency domain [4].

For this, the guard interval is included within the DFT interval while in CP-OFDM this does not occur, as can be deduced from figure 3.2. In addition, a very similar spectral

efficiency is achieved, because despite the introduction of said redundant subcarriers, the length of the UW-OFDM symbol can be defined shorter [4].

In spite of all the differences, both waveforms have in common that when performing the linear convolution of the OFDM symbol transmitted with the channel impulse response, a circular convolution is obtained in the receiver [3],[4],[5].

3.2.3 Generation

Unlike CP-OFDM, the generation of symbols in UW-OFDM is not so straightforward. As we have seen in figure 3.2, the UW-OFDM symbol consists of two parts: a guard interval, also called unique word, and data [5]. This symbol is defined in the time domain having a size N that matches the one of the DFT, and it can be defined as follows:

$$x^{'} = [\, x_d^T x_u^T]^{\,T} \tag{3.17}$$

Where $x_u \in \mathbb{C}^{N_u \times 1}$ represents the default sequence also known as unique word and $x_d \in \mathbb{C}^{(N-N_u)\times 1}$ represents the random data to be transmitted.

When generating these symbols, there are numerous alternatives, but the most widespread method is done in two steps [4]. First, a symbol with unique word 0 is generated in such a way that:

$$x = [\, x_d^T 0^T]^{\,T} \tag{3.18}$$

Subsequently, the desired unique word is added such that the UW-OFDM symbol is:

$$x^{'} = x + [\, 0^T x_u^T]^{\,T} \tag{3.19}$$

To understand it better, let's address the two steps separately. In the first step, it is necessary to obtain x, which is the data transmitted followed by the 0 unique word, both in the time domain. As in CP-OFDM, both the QAM symbols to be transmitted (given by $\bar{d} \in \mathbb{C}^{N_d \times 1}$) and the subcarriers used in the zero padding are given in the frequency domain [4]. Therefore, it is necessary to apply an IDFT to transform them to the time domain. If the data set and zero subcarriers are named as $\bar{x}$ and then, the IDFT $F_N^{-1}$is applied, then it is obtained that:

$$x = F_N^{-1}\bar{x} = [\, x_d^T 0^T]^{\,T} \tag{3.20}$$

To comply with the equations, a series of redundant subcarriers are introduced in frequency reducing the number of subcarriers used for data transmission. These redundant subcarriers form the vector $\bar{r} \in \mathbb{C}^{N_r \times 1}$ where $N_r = N_u$, which are distributed along the

spectrum using the permutation matrix $P \in \mathbb{C}^{(N_d+N_r)\times(N_d+N_r)}$ [4],[5]. The correct choice of P is crucial, since it can help to distribute the energy efficiently throughout the spectrum, thus reducing the PAPR.

With all this in mind, equality can be written as follows:

$$\bar{x} = BP \begin{bmatrix} \bar{d} \\ \bar{r} \end{bmatrix} \tag{3.21}$$

Where $B \in \mathbb{C}^{N\times(N_d+N_r)}$ is a matrix that introduces subcarriers belonging to zero padding. This matrix consists of zero rows in the positions where the zero padding is intended to be inserted and of unit rows in the positions where the data to be transmitted is (redundant subcarriers included).

If the N-IDFT is applied in order to convert the signal to the time domain, it is obtained:

$$x = F_N^{-1}\bar{x} = F_N^{-1}BP \begin{bmatrix} \bar{d} \\ \bar{r} \end{bmatrix} \tag{3.22}$$

And as it has been seen in the equation 3.20, this expression must be equal to:

$$F_N^{-1}BP \begin{bmatrix} \bar{d} \\ \bar{r} \end{bmatrix} = \begin{bmatrix} x_d \\ 0 \end{bmatrix} \tag{3.23}$$

From this expression, it can be assumed that:

$$F_N^{-1}BP = \begin{bmatrix} M_{11} & M_{12} \\ M_{21} & M_{22} \end{bmatrix} \tag{3.24}$$

Where $M \in \mathbb{C}^{N\times(N_d+N_r)}$, and the M_{ij} matrices with i, j with $i, j = 1, 2$ have the appropriate size. Starting from this equation, the relationships are established as:

$$M_{11}\bar{d} + M_{12}\bar{r} = x_d \tag{3.25}$$

$$M_{21}\bar{d} + M_{22}\bar{r} = 0 \tag{3.26}$$

From where it is derived that:

$$\bar{r} = -M_{22}^{-1}M_{21}\bar{d} \tag{3.27}$$

In order to simplify the equation 3.27, a matrix T is defined as follows:

$$T = -M_{22}^{-1} M_{21} \tag{3.28}$$

Where $T \in \mathbb{C}^{N_r \times N_d}$. Therefore, the equation 2.29 can be rewritten as:

$$\bar{r} = T\bar{d} \tag{3.29}$$

From this equation, it can be deduced that T introduces correlations in $\bar{x}$, and, therefore, its proper choice is of vital importance since it affects the energy of the redundant subcarriers $\bar{r}$. This can be observed from the equation that defines the average symbol energy:

$$E_x^{'} = \frac{1}{N}\left(N_d\sigma_d^2 + \sigma_d^2 tr(TT^H)\right) + x_u^H x_u \tag{3.30}$$

From here, it can be defined the next expressions:

$$E_{\bar{d}} = N_d\sigma_d^2 \tag{3.31}$$

$$E_{\bar{r}} = \sigma_d^2 tr(TT^H) \tag{3.32}$$

$$E_{x_u} = x_u^H x_u \tag{3.33}$$

Where E_{x_u} represents the contribution of the unique word to the average energy of the symbol, and $\frac{E_{\bar{r}}}{N}$ and $\frac{E_{\bar{d}}}{N}$ represent the contributions by the redundant subcarriers and the data before adding the unique word respectively [4],[5].

As can it be seen in the equation 3.32, the energy contributed by the redundant subcarriers can be very high if a bad choice of the matrix T is made. This relationship can also be established with P, since as we have seen in the equations 3.24 and 3.28, T depends on this permutation matrix. Therefore, it can be affirmed that a bad choice of P, such as $P = I$, can contribute with a very high level of energy by the redundant subcarriers [4],[5].

Therefore, it is necessary to choose a matrix P, or what is the same, a matrix T, which minimizes the cost function J of said energy. From the equation 3.30, this concept can be expressed as:

$$J_E = \frac{\sigma_d^2}{N} tr(TT^H) \tag{3.34}$$

In the equation 3.19, the symbol to be transmitted in the time domain is defined. However,

this expression is not entirely practical and therefore, another type of interpretation is made. [5]

It is assumed that:

$$G = P \begin{bmatrix} I \\ T \end{bmatrix} \tag{3.35}$$

Where $G \in \mathbb{C}^{(N_r+N_d)\times N_d}$ .If the equation above is used, then the equation 3.21 can be interpreted as:

$$\bar{c} = P \begin{bmatrix} \bar{d} \\ \bar{r} \end{bmatrix} = P \begin{bmatrix} I \\ T \end{bmatrix} \bar{d} = G\bar{d} \tag{3.36}$$

Where G and $\bar{c} \in \mathbb{C}^{(N_r+N_d)\times 1}$ represent a code generation matrix and a codeword of a systematic complex number Reed – Solomon code respectively. This fact can be seen graphically in the figure 3.3.

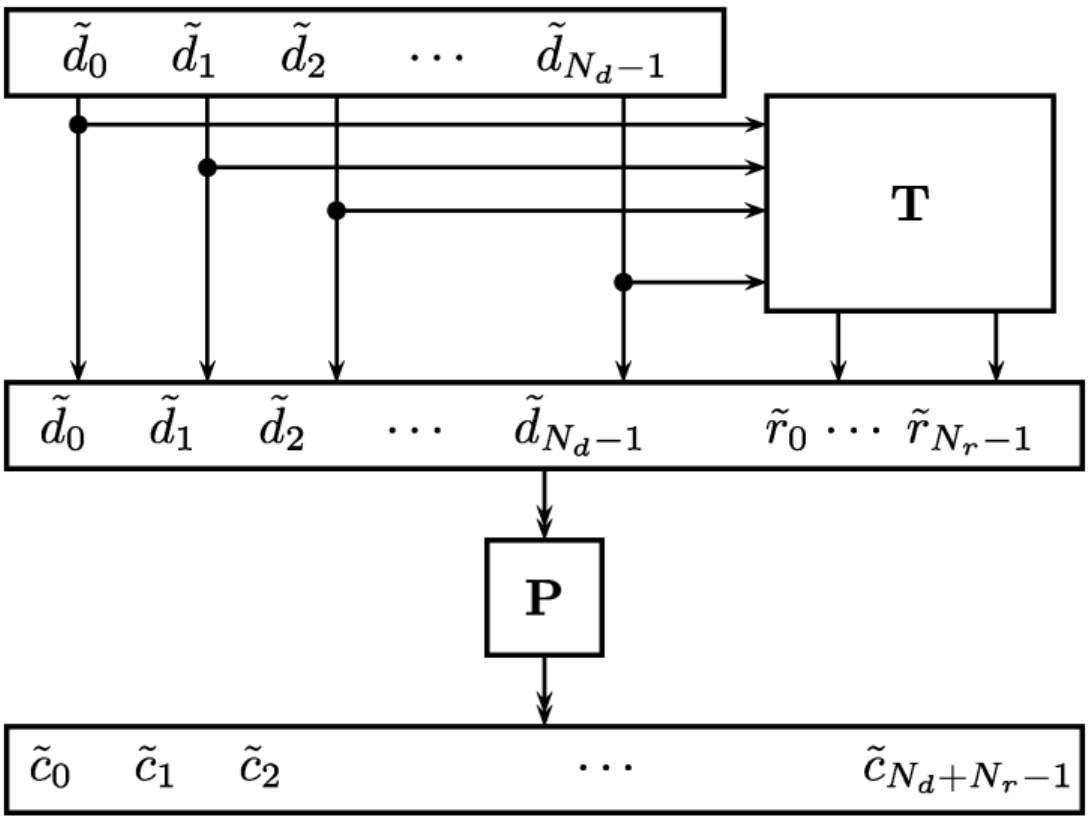

Figure 3.3. *Codeword generator for the systematic code described by G*
Fig. 3 [1]

By using the equations 3.21 and 3.35, it is obtained that:

$$\bar{x} = B\bar{c} \tag{3.37}$$

Therefore, x_u, which is the unique word defined in the frequency domain, can be expressed as:

$$\bar{x_u} = F_N[\ 0^T x_u^T]\ ^T \tag{3.38}$$

By using both equations 3.19 and 3.38, the equation 3.17, and therefore the transmitted UW-OFDM symbol in time domain, can be rewritten as:

$$x^{'} = x + [\ 0^T x_u^T]\ ^T \tag{3.39}$$

$$x^{'} = F_N^{-1}(B\bar{c} + \bar{x_u}) \tag{3.40}$$

$$x^{'} = F_N^{-1}(BG\bar{d} + \bar{x_u}) \tag{3.41}$$

This interpretation of the symbol $x^{'}$ is more appropriate to understand the operation of the complete system.

3.2.4 Receiver in UW-OFDM

In the previous section, it has been shown what is the expression that defines the UW-OFDM symbol to be transmitted. However, the effects of the channel and the equalization and decoding process of the received data have not been analyzed [3],[4],[5].

When a symbol is transmitted, it is affected, typically, by a multi-path channel and also by noise. Therefore, the received symbol in the time domain can be expressed as:

$$y_r = H_c x^{'} + n \tag{3.42}$$

Where $H_c \in \mathbb{C}^{N\times N}$ represents a cyclic convolution matrix obtained from the vector containing the channel impulse response coefficients $h \in \mathbb{C}^{N\times 1}$ with zero padding and $n \in \mathbb{C}^{N\times 1}$ represents the zero-mean Gaussian noise vector with $\sigma_n^2 I$ as the covariance matrix [3],[4],[5]. The next step is to go from time domain to frequency domain through the DFT. Following this process, those subcarriers that introduced zeros into the transmitter

can be extracted, obtaining:

$$\bar{y_d} = B^T F_N y_r = B^T F_N H_c x^{'} + B^T F_N n = B^T F_N H_c F_N^{-1}(BG\bar{d} + \bar{x_u}) + B^T F_N n \quad (3.43)$$

From the previous equation, the matrix $\bar{H_c}$ can be obtained as follows:

$$\bar{H_c} = F_N H_c F_N^{-1} \quad (3.44)$$

$\bar{H_c}$ is a diagonal matrix whose, regardless of redundancy, diagonal contains the sampled channel frequency response [4]. If the zero padding is also eliminated, then the matrix $\bar{H}$ is obtained, which can be expressed as:

$$\bar{H} = B^T \bar{H_c} B = B^T F_N H F_N^{-1} B \quad (3.45)$$

This matrix has on its diagonal the same coefficients of the frequency channel response as $\bar{H_c}$. If the equation 3.45 is used in the equation 3.43, it is obtained that:

$$\bar{y_d} = \bar{H}G\bar{d} + \bar{H}B^T\bar{x_u} + B^T F_N n \quad (3.46)$$

Assuming that $\bar{H}$ is known or, if not, it is possible to estimate it [4], then it can be differentiated two parts within the transmitted symbol. On the one hand, there is the unknown part associated with the data, $\bar{H}G\bar{d}$; and on the other hand, there is $\bar{H}B^T\bar{x_u}$, which is the known part of the symbol, since the unique word x_u was predefined. Finally, $B^T F_N n$ forms the noise vector.

In the next step, it is necessary to extract the influence of the unique word as follows:

$$\bar{y} = \bar{y_d} - HB^T\bar{x_u} \quad (3.47)$$

Once this is done, it is necessary to equalize $\bar{y}$ to obtain the linear estimate of the transmitted data $\bar{d}$. For this, it is necessary to obtain an E equalizer so that:

$$\hat{d} = E\bar{y} \quad (3.48)$$

3.2.5 Linear channel estimators for UW-OFDM

There are different approaches when establishing an appropriate linear estimator for unique word. As explained in [3], there are two ways to address it.

First, it can be assumed that the data is an unknown vector but at the same time is

deterministic. In this case and as stated in [3], the best linear unbiased estimator (BLUE) is obtained which is equivalent to a zero forcing equalizer of the form:

$$E_{BLUE} = (G^H \bar{H}^H \bar{H} G)^{-1} G^H \bar{H}^H \tag{3.49}$$

With an error covariance matrix:

$$C_{\bar{e}\bar{e}} = N\sigma_n^2 (G^H \bar{H}^H \bar{H} G)^{-1} \tag{3.50}$$

On the other hand, it can be assumed that the data is not deterministic, but rather is random. In this case, an linear minimum mean square error estimator (LMMSE) is obtained such that:

$$E_{LMMSE} = (G^H \bar{H}^H \bar{H} G + \frac{N\sigma_n^2}{\sigma_d^2} I)^{-1} G^H \bar{H}^H \tag{3.51}$$

With an error covariance matrix:

$$C_{\bar{e}\bar{e}} = N\sigma_n^2 (G^H \bar{H}^H \bar{H} G + \frac{N\sigma_n^2}{\sigma_d^2} I)^{-1} \tag{3.52}$$

As it can be seen, the expressions are practically the same as in the previous case, but in this occasion, the influence of noise and data are taken into account.

3.2.6 Non-systematic coding in UW-OFDM

By generating the UW-OFDM symbol, the power of the redundant subcarriers was minimized after minimizing the cost function J_E. In this way, the energy was distributed among all the redundant subcarriers, which in turn means to spread it among the entire codeword $\bar{c}$, avoiding the concentration of the energy in only certain subcarriers [4],[5].

However, there are different techniques that can minimize such energy even more. Among these techniques, there is non-systematic coding [3]. This process consists of distributing the energy not only among the redundant subcarriers, but also among the rest of the subcarriers. In this way, the energy is distributed equally among the different subcarriers.

In equation 3.36 it has been shown how codeword $\bar{c}$ is generated. Similarly, the codeword in the non-systematic coding is generated such that:

$$\bar{c} = \check{G}\bar{d} \tag{3.53}$$

Where $\check{G}$ is the code generation matrix that distributes the energy as explained above for the case of non-systematic coding [3]. This matrix $\check{G}$ is generated in a similar way to the

generating matrix G that it has been explained previously, but in this case, in addition to taking into account the distribution of the redundant energy, the complete communication system, receiver included, is taken into acccount.

As explained in [3], the cost functions of both the BLUE case and the LMMSE case are equal to the previous case where it was not considered non-systematic coding. Therefore, it is straightforward that changing G with $\check{G}$ is the only step needed. However, when optimizing $\check{G}$ it is not so obvious and the steps to do so are different.

The solution proposed in [3], consists of several steps. In the first, the steepest decent algorithm is applied to solve the optimization problems of [3]. With this in mind and taking equation 3.35, $\check{G}$ can be rewritten such that:

$$\check{G} = AP \begin{bmatrix} I \\ \check{T} \end{bmatrix} \tag{3.54}$$

The equation is practically identical to the one of the previous case, but the concept of the non-singular real matrix $A \in \mathbb{C}^{(N_d+N_r)\times(N_d+N_r)}$ is introduced. If the IFFT and the zero padding is introduced to this matrix, then it can be rewritten such that:

$$F_N^{-1} B\check{G} = F_N^{-1} BAP \begin{bmatrix} I \\ \check{T} \end{bmatrix} = \begin{bmatrix} W \\ 0 \end{bmatrix} \tag{3.55}$$

Similarly, equation 3.24 can be rewritten such that:

$$\check{M} = F_N^{-1} BAP \begin{bmatrix} \check{M}_{11} & \check{M}_{12} \\ \check{M}_{21} & \check{M}_{22} \end{bmatrix} \tag{3.56}$$

From where, $\check{T}$ can be obtained as:

$$\check{T} = -\check{M}_{22}{}^{-1} \check{M}_{21} \tag{3.57}$$

Therefore, it can be concluded that from a given matrix A, the matrices $\check{G}$ and $\check{T}$ that minimize the aforementioned cost functions can be obtained [3]. Therefore, it can be affirmed that, to obtain an optimal matrix A, some of the cost functions must be minimal:

$$A_{opt} = argmin\ J_{BLUE}, J_{LMMSE} \tag{3.58}$$

The steepest descent algorithm consists in taking the gradient of the cost function J with

respect to the matrix A in order to find said A_{opt}. This is expressed such that:

$$\frac{\partial J}{\partial [A]_{ij}} = \frac{J(|A|_{ij} + \epsilon) - J(|A|_{ij} - \epsilon)}{2\epsilon} \tag{3.59}$$

Once said A_{opt} is obtained, a matrix $\check{G}$ is obtained from a set of matrices that meet the requirement of equation 3.54 to obtain a unique word 0. In order to understand this process better, it is necessary to understand how to apply the steepest descent algorithm.

There are two ways to initialize the algorithm. The first of the recommendations, as mentioned in [3], is to use the identity matrix I. Therefore, it is straightforward that the initial value of $\check{T}$ will also be T, and, in turn, $\check{G}$ will have an equal initial value to G.

On the other hand, there is a random initialization, which consists in assigning to each element of the matrix A the value of a Gaussian random variable of mean zero and variance 1 [3].

3.2.7 Disadvantages of UW-OFDM

Despite the numerous advantages that UW-OFDM offers over CP-OFDM, there are also certain disadvantages. On the one hand, it is found an increase in terms of complexity when generating the UW-OFDM symbol [4].

In CP-OFDM, the process of generating the symbol was rather simple. IFFT is applied to the data, the cyclic prefix is then added and the pulse shape filter is applied. However, in UW-OFDM the data is affected by many more changes. On the one hand, redundant subcarriers are added through the use of the generating matrix G [3].

In addition, because a unique word is added, the receiver has to use more complex equalizers [5]. Not only this problem appaers, but also it can be added that minimizing the cost function to find the optimal matrices is a slow process compared to CP-OFDM.

Finally, the main downside is the fact that all the papers and implementations dealing with UW-OFDM consider a channel whose channel impulse response' coefficients are known [3],[4],[5]. This is somehow unrealistic, since a real channel is random and with a multipath fading effect. This turns to be even more serious for the MIMO case, since there is not only one assumption, but all possible paths are assumed.

4 RESULTS

4.1 Introduction

As mentioned above, the goal of this thesis is to analyze the throughput of CP-OFDM in high velocity use cases with 5G NR technology, testing different configurations, and its comparison with UW-OFDM. All these objectives are being sought by using the MATLAB toolbox for 5G. All the different experiments that have been performed will be mentioned individually below.

It is worth highlighting certain parameters that have been fixed for the different experiments. The number of sent frames has always been 100, there are 8 transmitting antennas and 2 receiving antennas, as well as 64-QAM has been the modulation used. In addition, in the case of CP-OFDM, DMRS symbol position equal to 2, DMRS configuration type equal to 1, a clustered delay line (CDL) channel type is assumed and a 50 MHz bandwidth has been selected. In addition, a perfect synchronization and therefore all the signals related to synchronization, have been eliminated, increasing the number of RBs that transmit data.

In the case of the channel, a CDL-D type has been chosen since it is more suited to an urban environment, which is the main application area of 5G. This channel has been chosen respecting the specifications, and therefore, a K-factor equal to 7 and a K-factor of the first cluster equal to 13.3 have been chosen. In addition, the root-mean-squared delay spread has been established at 300ns, which is a value within typical ranges.

It has been decided not to use some of the typical functions of the toolbox when performing the channel estimation, since they only work for a certain combination of parameters and they are not tested for all the possible scenarios. Therefore, it has been decided to use DMRS symbols in order to estimate the channel by interpolation, both in time and frequency.

However, there are other parameters that vary depending on the different comparatives. The subcarrier spacing, the carrier frequency, the device's speed, the number of DMRS symbols and the tested waveform are the main parameters that will change.

4.2 DMRS test

The first test consists in analyzing the effect that the variation of the number of DMRS symbols has on the throughput.

- Scenario 1:
  - SCS = 60 kHz
  - f_c = 3.5 GHz
  - v = 3 km/h

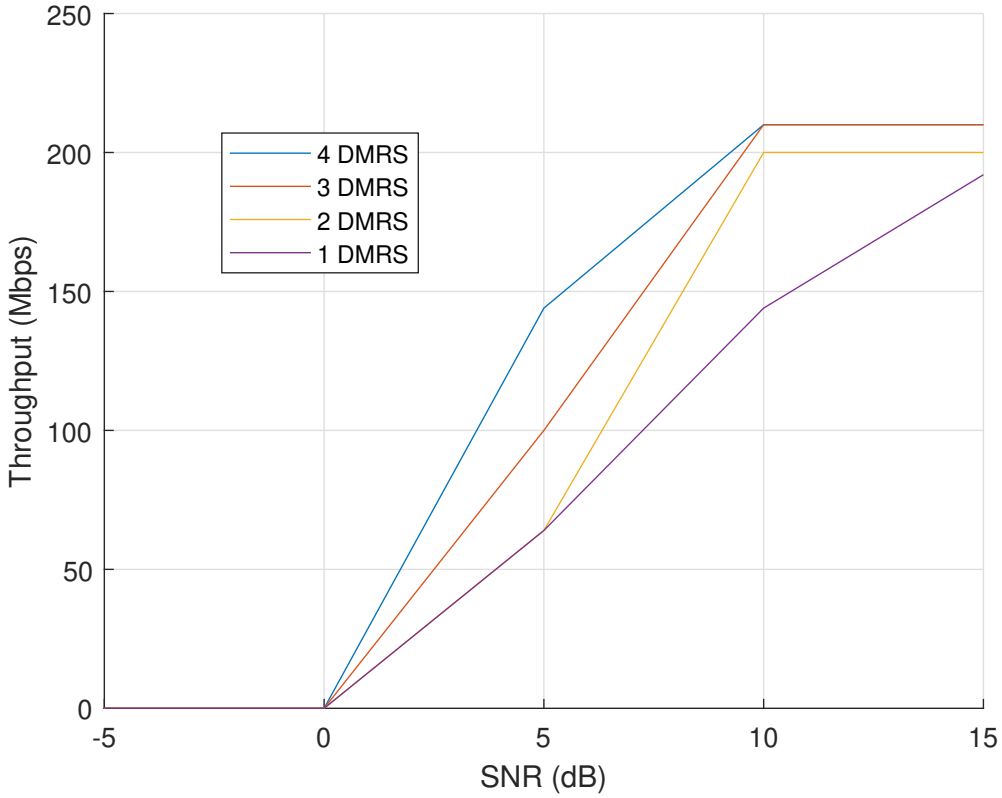

Figure 4.1. *Evolution of throughput in scenario 1*

As it can be seen in the figure, adding more DMRS symbols improves the total throughput as expected. By adding more DMRS symbols, there is less distance between two consecutive DMRS symbols, and therefore, when the interpolation is done, the channel estimation is better as fast time variations can be estimated more precisely.

In the case where there is only one DMRS symbol, this cannot be done, and therefore, the only DMRS symbol's value is extended over all other symbols in time, making interpolation only in the frequency domain. This is the less precise channel estimation that can be done, so therefore, the throughput for 1 DMRS symbol is the smaller one.

This effect can be also seen at other velocities as shown in the figures 4.2 and 4.3.

- Scenario 2:
  - SCS = 60 kHz
  - f_c = 3.5 GHz
  - v = 160 km/h

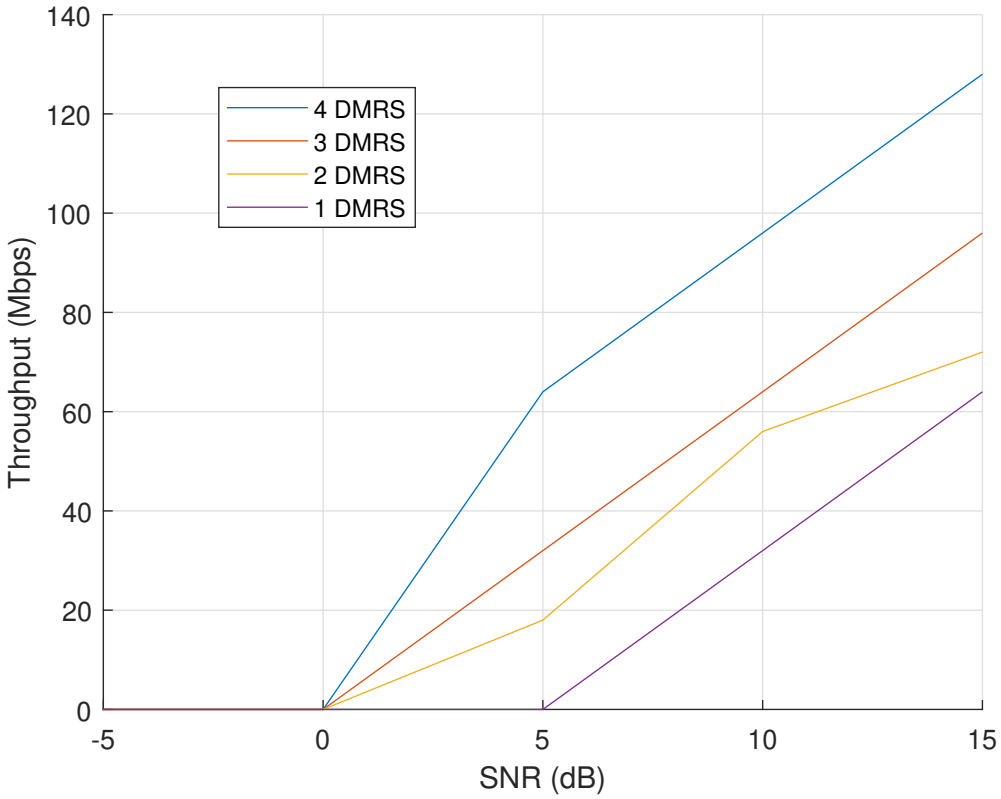

Figure 4.2. *Evolution of throughput in scenario 2*

As it can be seen for every velocity, using a small number of DMRS symbols affects the channel estimation, and therefore, the throughput decreases as a consequence of a non correct channel estimation. Furthermore, it can be seen that for high speed scenarios, the effect of using a small number of these DMRS symbols is even more important, as it can reach throughput 0.

Using only one DMRS symbol is not enough when the Doppler shift is so high as for the high speed devices, as the coherence time (which is the period of time over which channel time-domain variations do not have such a big influence) is smaller. This means, that for higher velocities, the channel is more varying so it is more difficult to estimate it. Also, by having a higher Doppler shift, a higher ICI will be generated, which also affects the channel estimation.

That is why a greater number of DMRS symbols is needed, as it improves the channel estimation, and because of that, it also increases the throughput.

- Scenario 3:
  - SCS = 60 kHz
  - f_c = 3.5 GHz
  - v = 240 km/h

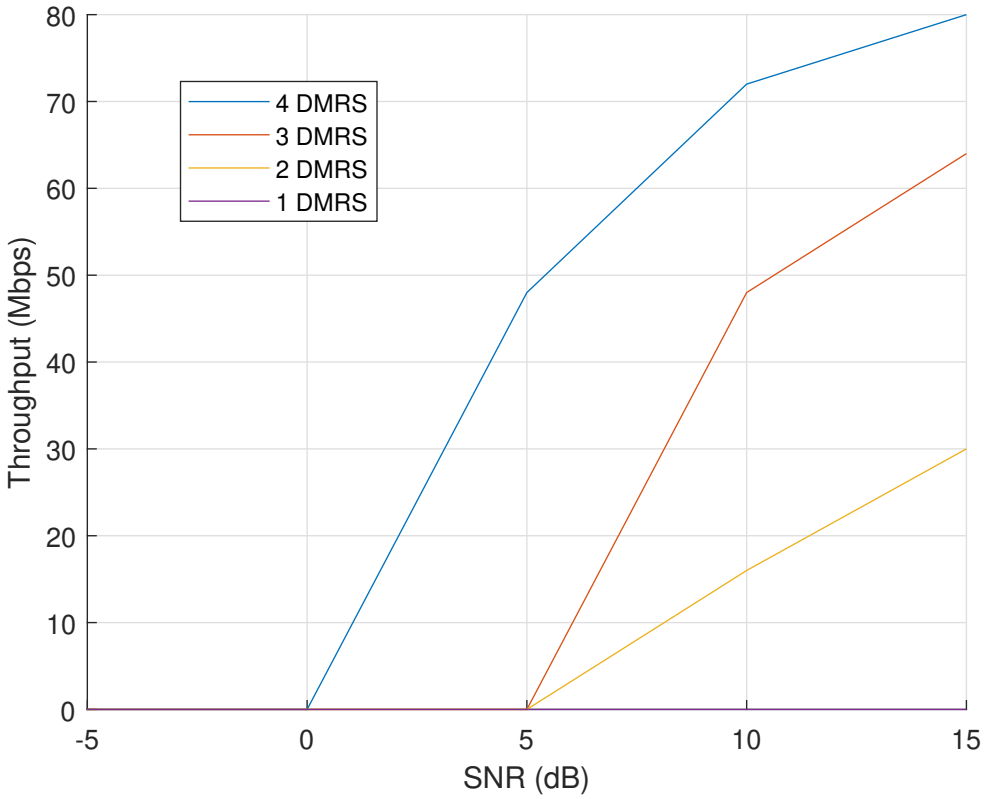

Figure 4.3. *Evolution of throughput in scenario 3*

4.3 Velocity test

The second experiment consists in analyzing how the throughput is affected by the speed at which a device moves. In this case, the chosen speeds are 3, 160 and 240 km/h. The speed is one of the parameters that affects the Doppler shift, which is an effect that has a big influence in the throughput. The Doppler shift can be defined as:

$$\Delta f_{Doppler} = \frac{v}{c} f_c \tag{4.1}$$

- Scenario 4:
  - SCS = 60 kHz
  - f_c = 3.5 GHz
  - $DMRS$ = 4

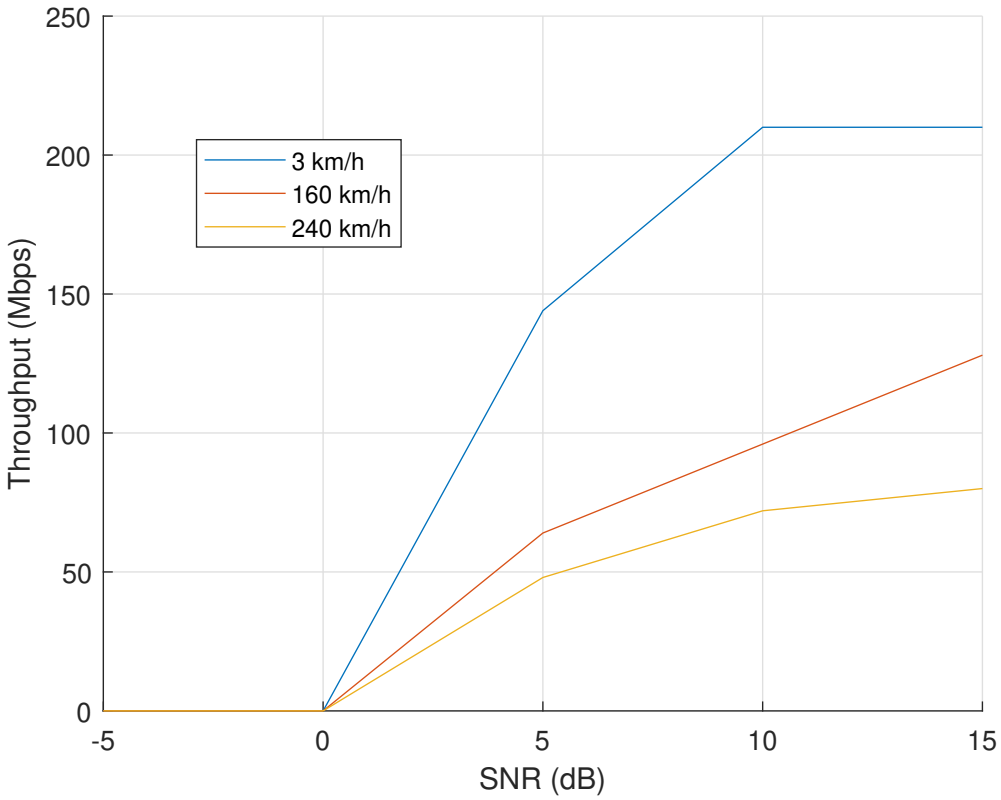

Figure 4.4. *Evolution of throughput in scenario 4*

The first information that can be extracted from figures 4.4 and 4.5, is that for high velocities, the throughput decreases significantly. This is so, because the Doppler shift depends on the speed, and as it increases, the Doppler shift also increases. As it has been explained in the previous test, this affects the channel, which is more varying and because of that, its estimation becomes more difficult. And also, by having a higher Doppler shift there is more ICI introduced between consecutive subcarriers.

As it can be seen for both scenarios, a low speed such as 3 km/h generates a practically non-varying channel, which makes the throughput to be practically maximum. On the other hand, for higher speeds scenarios, such as for 160 or 240 km/h, the Doppler shift increases significantly, so the channel becomes less easier to estimate. Therefore, for higher speeds the throughput will decrease as expected.

The subcarrier spacing is also affecting the total throughput as it can be observed in the figures. This happens because, for a higher SCS and a certain Doppler shift level, this Doppler shift represents a smaller percentage of the bandwidth of the subcarrier than for smaller SCS. Therefore, the ICI is smaller, increasing the total throughput.

- Scenario 5:
  - SCS = 15 kHz
  - f_c = 3.5 GHz
  - $DMRS$ = 4

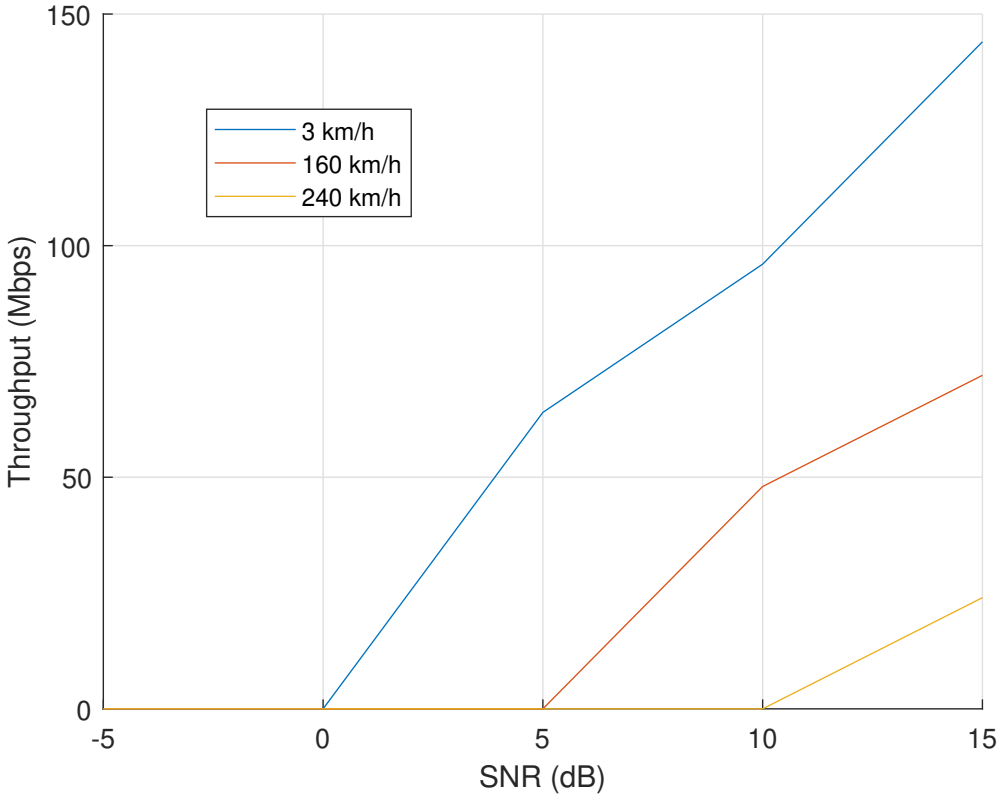

Figure 4.5. *Evolution of throughput in scenario 5*

From equation 3.1, it can be extracted that the Doppler shift is not only affected by the speed but also by the carrier frequency. For the scenarios selected, the Doppler shift can be computed by using the same equation:

- Doppler shift in scenarios 4 and 5:
  - $\Delta f_{Doppler3km/h}$ = 9.72 Hz
  - $\Delta f_{Doppler160km/h}$ = 518.52 Hz
  - $\Delta f_{Doppler240km/h}$ = 777.78 Hz

The Doppler shift is the same for both scenarios, but the throughput is lower for the 15 kHz SCS. This is due to the higher ICI introduced for this scenario, as the Doppler shift affects more the neighbor subcarriers as it has been explained earlier. This can be better understood if the percentage of SCS that the Doppler shift represents for each case is analyzed.

- Scenario 4:
  - $\%SCS_{3km/h} = \frac{9.72}{60000} \cdot 100 = 0.0162\%$
  - $\%SCS_{160km/h} = \frac{518.52}{60000} \cdot 100 = 0.8642\%$
  - $\%SCS_{240km/h} = \frac{777.78}{60000} \cdot 100 = 1.2963\%$
- Scenario 5:
  - $\%SCS_{3km/h} = \frac{9.72}{15000} \cdot 100 = 0.0648\%$
  - $\%SCS_{160km/h} = \frac{518.52}{15000} \cdot 100 = 3.4568\%$
  - $\%SCS_{240km/h} = \frac{777.78}{15000} \cdot 100 = 5.1852\%$

As it can be seen, the Doppler shift represents a higher percentage of the subcarrier's bandwidth when using smaller SCS, and because of that, a higher portion of the subcarrier's bandwidth is affected by its neighbors. Thus, there appears a higher ICI and, therefore, the throughput is smaller than in the previous scenario.

A higher ICI is not the only downside that using a smaller SCS has. As it has been explained before, by using a higher subcarrier spacing, the duration of the OFDM symbols is smaller, and therefore, for the same amount of time there will be more DMRS symbols than for a smaller subcarrier spacing. And as there are more DMRS symbols, the interpolation used for the channel estimation will be more precise, deriving in a greater throughput and a smaller error rate.

4.4 Carrier frequency test

Speed is not the only parameter that affects the Doppler shift. The carrier frequency also influences it as it can be extracted from the equation 3.1. Therefore, two different carrier frequencies, 3.5 GHz and 30 GHz, will be analyzed for three different speeds. These carrier frequencies values are selected as they are in the frequency ranges defined for 5G as seen in table 2.3.

As it can be extracted from figures 4.6, 4.7 and 4.8, increasing the carrier frequency from 3.5 to 30 GHz increases enormously the Doppler shift. Therefore, the behaviour is quite similar as in the velocity test. As it can be observed, for the three velocities, by using a higher carrier frequency the throughput decreases significantly, as a higher Doppler shift introduces more ICI.

- Scenario 6:
  - SCS = 60 kHz
  - v = 3 km/h
  - $DMRS$ = 4

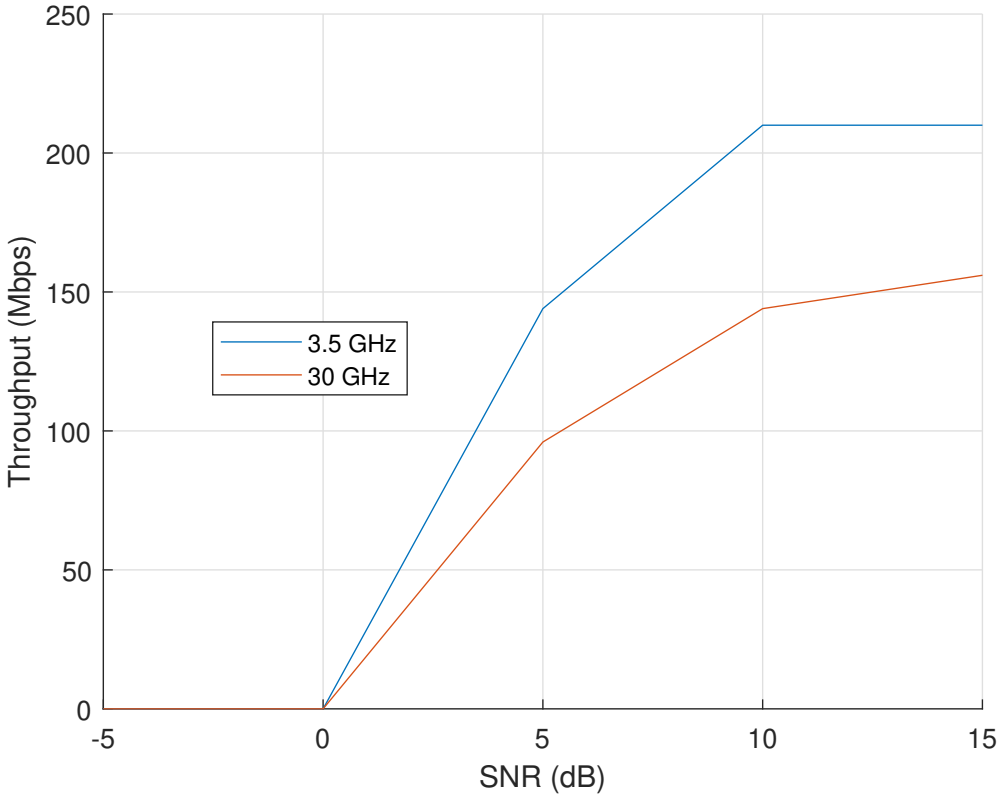

Figure 4.6. *Evolution of throughput in scenario 6*

- Scenario 7:
  - SCS = 60 kHz
  - v = 160 km/h
  - $DMRS$ = 4

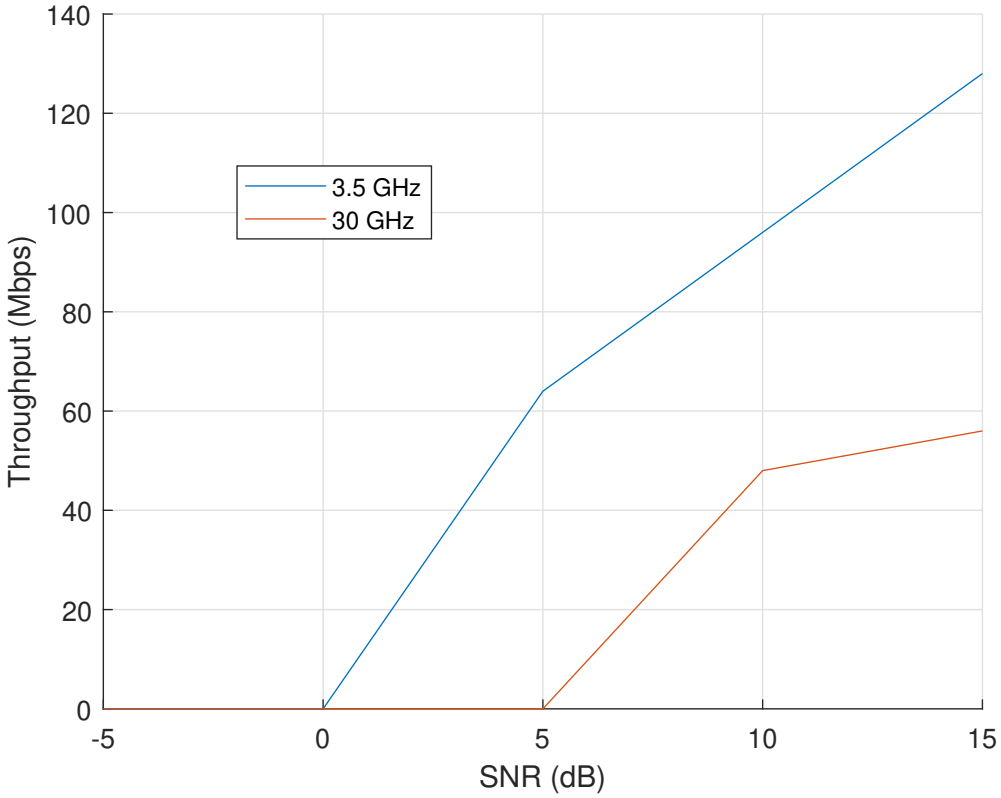

Figure 4.7. *Evolution of throughput in scenario 7*

- Scenario 8:
  - SCS = 60 kHz
  - v = 240 km/h
  - $DMRS$ = 4

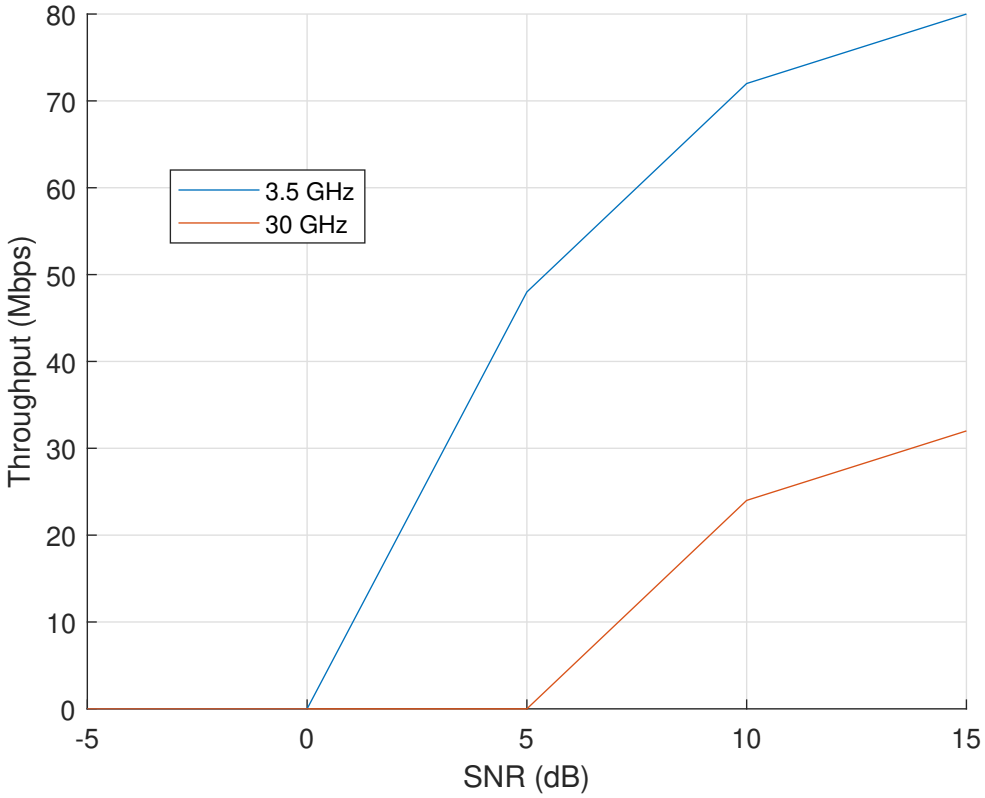

Figure 4.8. *Evolution of throughput in scenario 8*

In order to understand better the effect the carrier frequency has on the Doppler shift, and therefore, on the throughput, the Doppler shift will be computed for the three scenarios:

- Doppler shift in scenario 6:
  - $\Delta f_{Doppler3.5GHz}$ = 9.72 Hz
  - $\Delta f_{Doppler30GHz}$ = 83.33 Hz
- Doppler shift in scenario 7:
  - $\Delta f_{Doppler3.5GHz}$ = 518.52 Hz
  - $\Delta f_{Doppler30GHz}$ = 4.44 kHz
- Doppler shift in scenario 8:
  - $\Delta f_{Doppler3.5GHz}$ = 777.78 Hz
  - $\Delta f_{Doppler30GHz}$ = 6.67 kHz

As it can be seen, the Doppler shift increases significantly when increasing the carrier frequency, introducing more ICI between neighbors subcarriers. The amount of bandwidth affected is higher in the case of the higher carrier frequency, as the Doppler shift is greater. The Doppler shifts generated by both frequency ranges represent the following percentages of the SCS of 60 kHz:

- Scenario 6:
  - $\%SCS_{3.5GHz} = \frac{9.72}{60000} \cdot 100 = 0.0162\%$
  - $\%SCS_{30GHz} = \frac{83.33}{60000} \cdot 100 = 0.1389\%$
- Scenario 7:
  - $\%SCS_{3.5GHz} = \frac{518.52}{60000} \cdot 100 = 0.8642\%$
  - $\%SCS_{30GHz} = \frac{4.44}{60} \cdot 100 = 7.4\%$
- Scenario 8:
  - $\%SCS_{3.5GHz} = \frac{777.78}{60000} \cdot 100 = 1.2963\%$
  - $\%SCS_{30GHz} = \frac{6.67}{60} \cdot 100 = 11.12\%$

As expected, when having a higher Doppler shift, the percentage of subcarrier's bandwidth affected by the neighbors subcarriers increases. For example, for scenario 8, there is a 10 times increment in terms of bandwidth affected by the Doppler shift. This is a huge difference, and therefore, as it has been shown in the previous figures, the total throughput decays significantly.

4.5 Subcarrier spacing test

The last parameter that is going to be analyzed is the subcarrier spacing. Even though its effect on the throughput has been analyzed in the velocity test, more scenarios are going to be taken into account. The importance of the subcarrier's spacing effect on the throughput resides, as it has been already analyzed, in the total subcarrier's bandwidth portion that is affected by the Doppler shift.

As it can be seen in figures 4.9, 4.10 and 4.11, when increasing the SCS, the throughput also increases. This effect has been analyzed in the previous tests, and it has been stated that a fixed Doppler shift, represents a smaller percentage of the total subcarrier's bandwidth when the SCS is greater. Because of this, the ICI introduced is smaller, and therefore, the throughput increases.

- Scenario 9:
  - f_c = 3.5 GHz
  - v = 3 km/h
  - $DMRS$ = 4

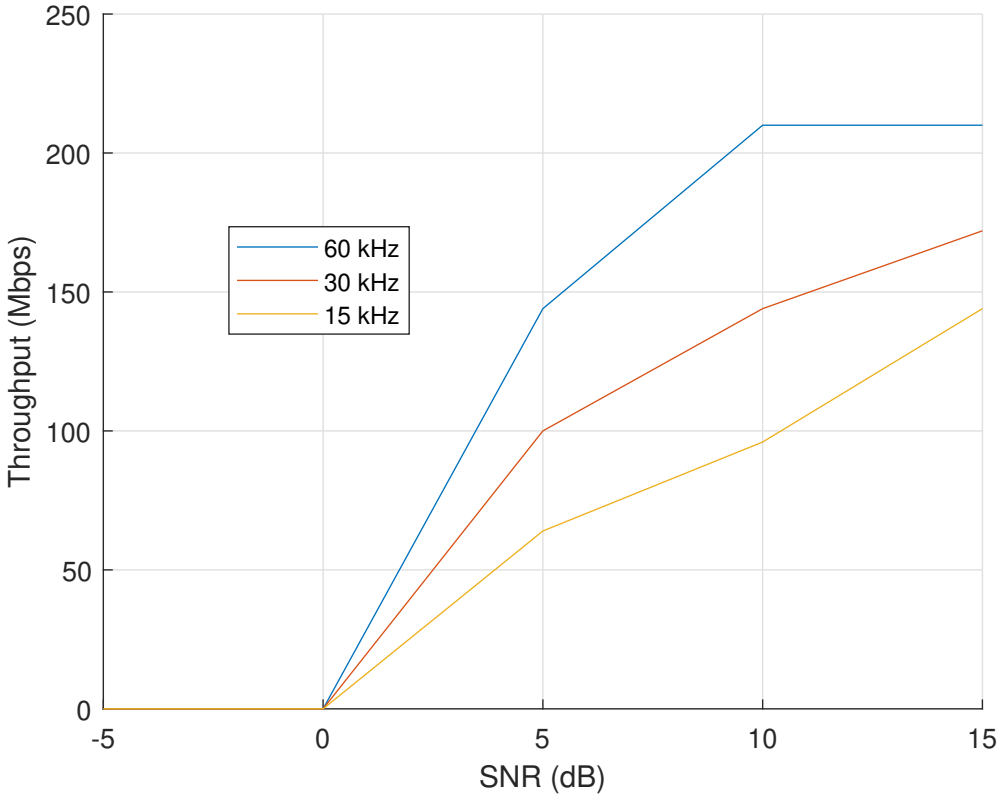

Figure 4.9. *Evolution of throughput in scenario 9*

- Scenario 10:
  - f_c = 3.5 GHz
  - v = 160 km/h
  - $DMRS$ = 4

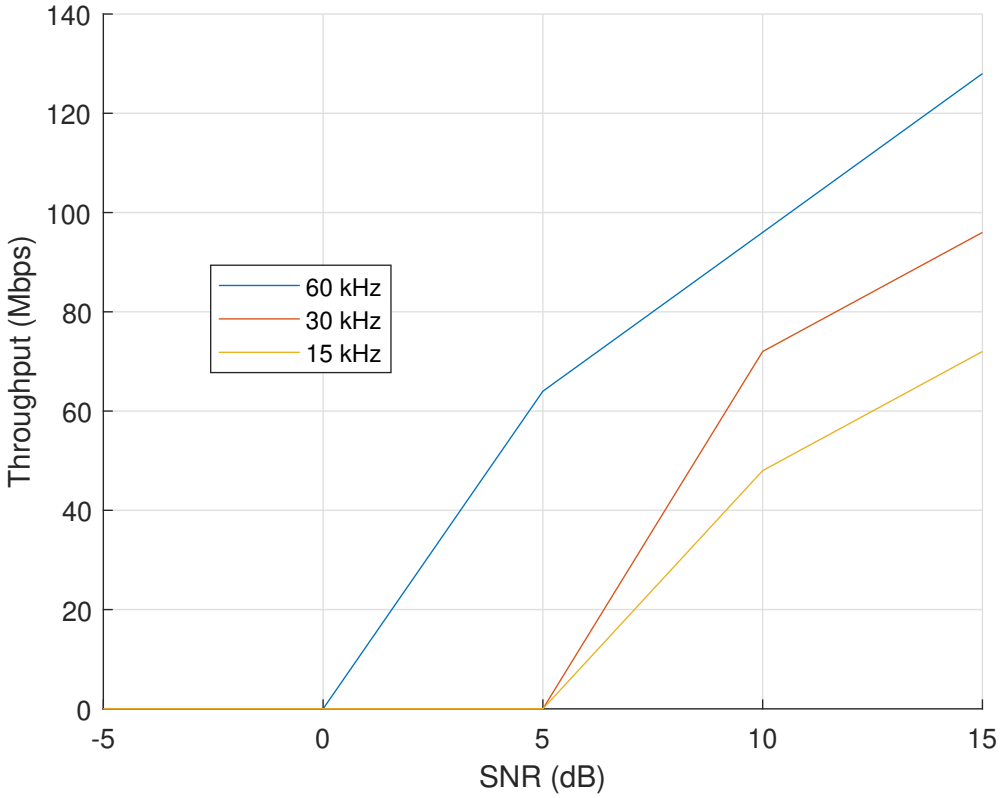

Figure 4.10. *Evolution of throughput in scenario 10*

- Scenario 11:
  - f_c = 3.5 GHz
  - v = 240 km/h
  - $DMRS$ = 4

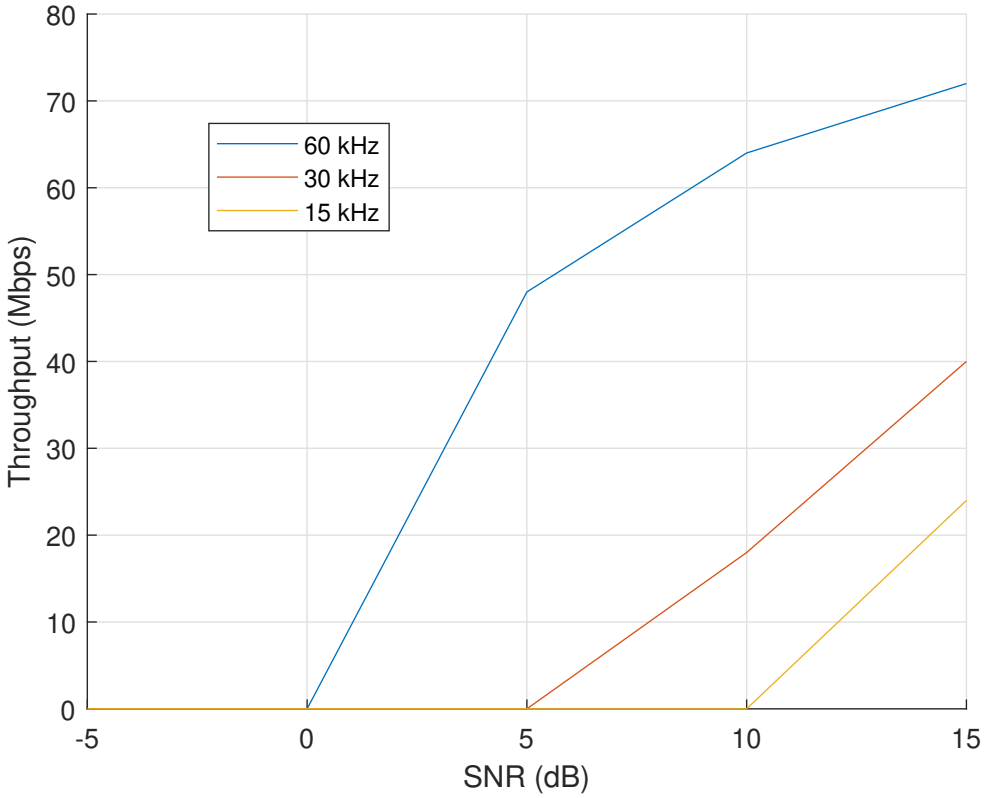

Figure 4.11. *Evolution of throughput in scenario 11*

- Scenario 9:
  - $\%SCS_{15kHz} = \frac{9.72}{15000} \cdot 100 = 0.0648\%$
  - $\%SCS_{30kHz} = \frac{9.72}{30000} \cdot 100 = 0.0324\%$
  - $\%SCS_{60kHz} = \frac{9.72}{60000} \cdot 100 = 0.0162\%$
- Scenario 10:
  - $\%SCS_{15kHz} = \frac{518.52}{15000} \cdot 100 = 3.4568\%$
  - $\%SCS_{30kHz} = \frac{518.52}{30000} \cdot 100 = 1.7284\%$
  - $\%SCS_{60kHz} = \frac{518.52}{60000} \cdot 100 = 0.8642\%$
- Scenario 11:
  - $\%SCS_{15kHz} = \frac{777.78}{15000} \cdot 100 = 5.1852\%$
  - $\%SCS_{30kHz} = \frac{777.78}{30000} \cdot 100 = 2.5926\%$
  - $\%SCS_{60kHz} = \frac{777.78}{60000} \cdot 100 = 1.2963\%$

If we analyze the percentages of the subcarrier's bandwidth that the Doppler shift represents, it can be confirmed that, for higher SCS, the effect of this Doppler shift is smaller. Also, as mentioned in the DMRS test, when having a higher SCS, the duration of the OFDM symbols is reduced. Therefore, for the same amount of time, there are going to be more DMRS symbols in a high SCS scenario than in a small SCS scenario. This will cause, as mentioned, a better channel estimation, and furthermore, a higher throughput.

4.6 CP-OFDM vs UW-OFDM

Finally, the last comparison is made between the two waveforms: CP-OFDM and UW-OFDM. As mentioned above, one of the main problems of UW-OFDM is that the channel is assumed to be known [1],[2],[3]. The studies carried out do not establish a procedure to estimate the channel using the unique word nor any other procedures. Therefore, for the comparison, the same channel has been used for both CP-OFDM and UW-OFDM, whose coefficients are established previously, in a SISO scenario. In order to compare both waveforms, different scenarios have been analyzed.

- Scenario 1:
  - SCS = 60 kHz
  - f_c = 3.5 GHz
  - v = 3 km/h

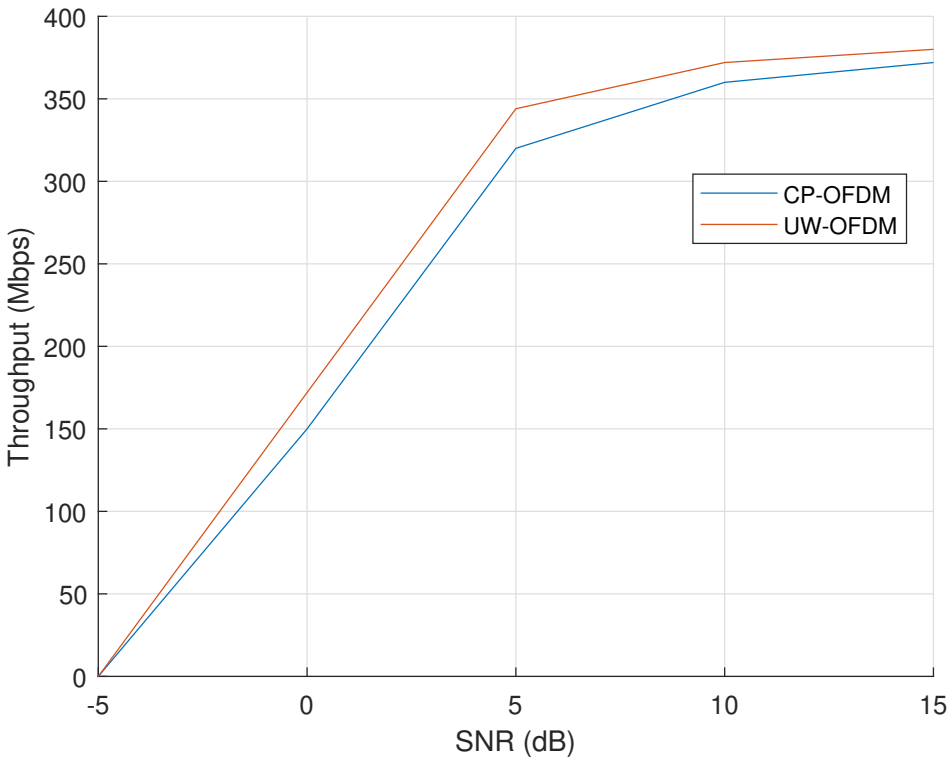

Figure 4.12. *Comparison of CP-OFDM and UW-OFDM in scenario 1*

- Scenario 2:
  - SCS = 60 kHz
  - f_c = 3.5 GHz
  - v = 160 km/h

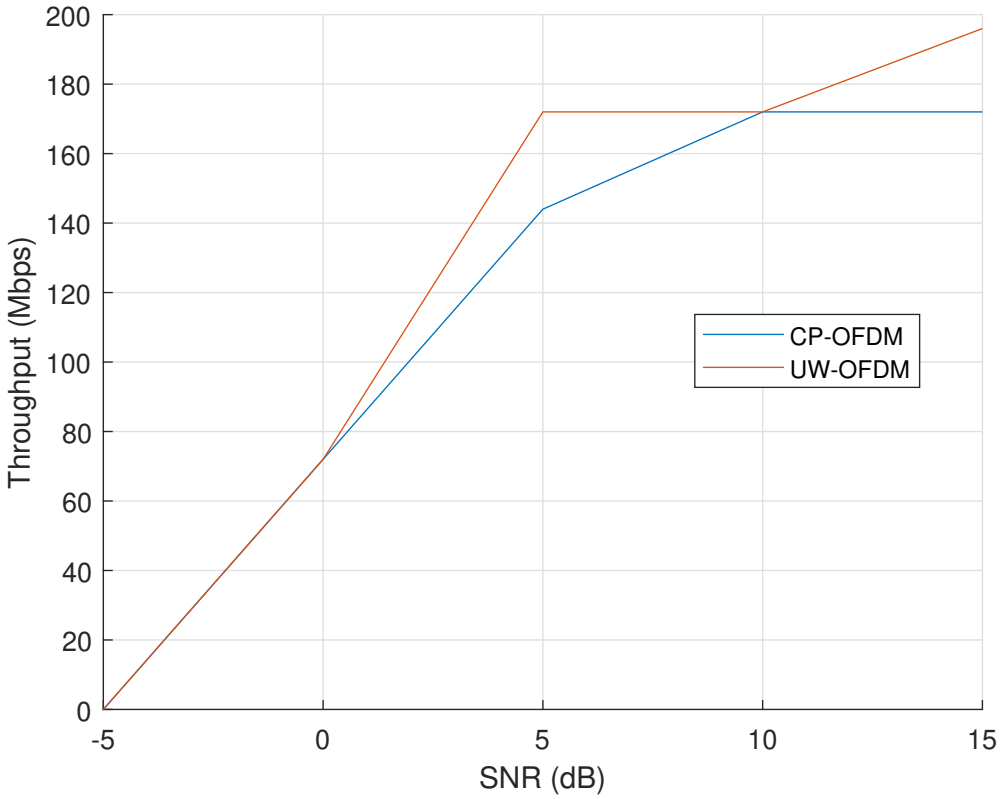

Figure 4.13. *Comparison of CP-OFDM and UW-OFDM in scenario 2*

- Scenario 3:
  - SCS = 60 kHz
  - f_c = 3.5 GHz
  - v = 240 km/h

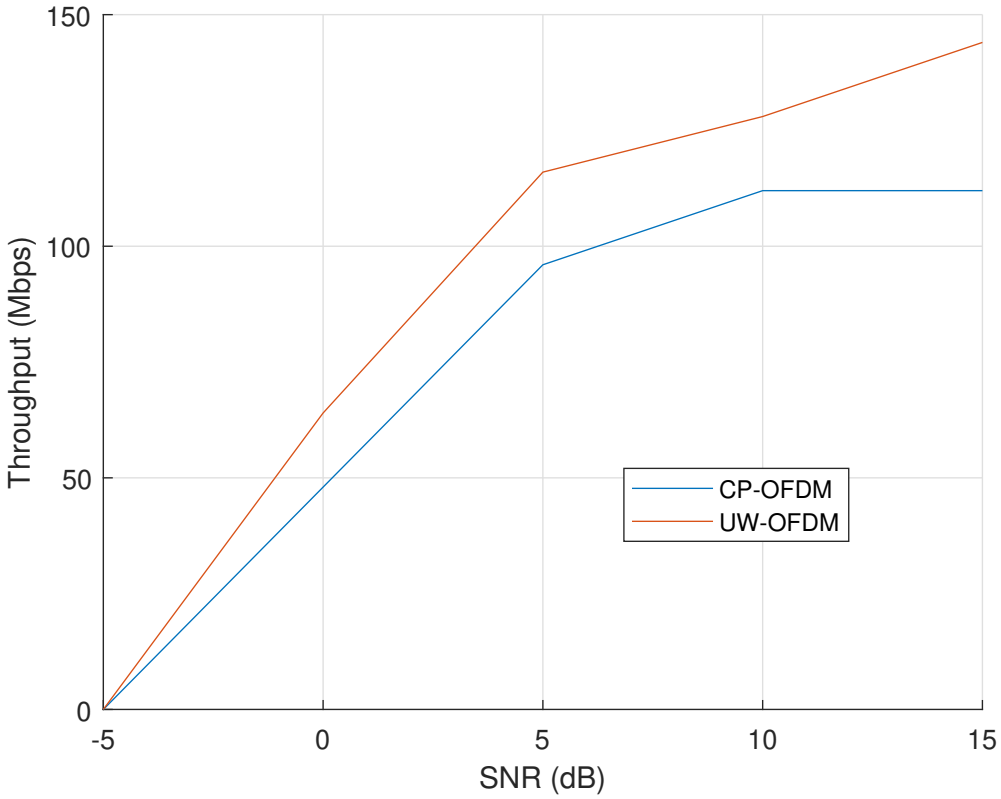

Figure 4.14. *Comparison of CP-OFDM and UW-OFDM in scenario 3*

- Scenario 4:
  - SCS = 30 kHz
  - f_c = 3.5 GHz
  - v = 160 km/h

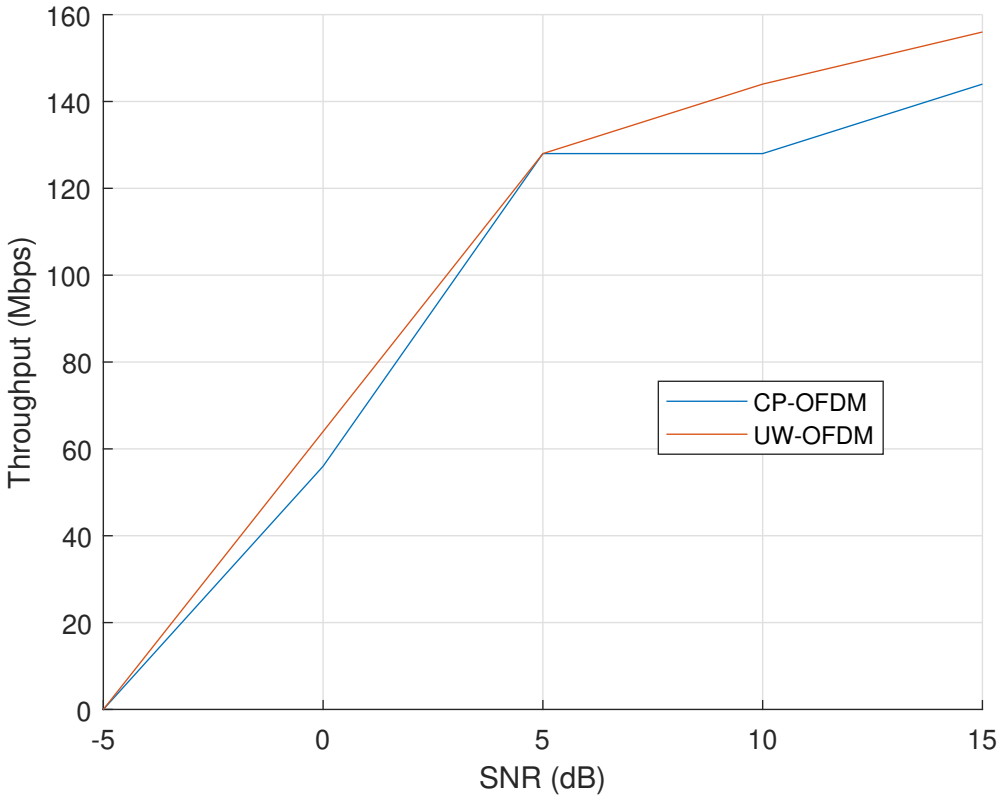

Figure 4.15. *Comparison of CP-OFDM and UW-OFDM in scenario 4*

- Scenario 5:
  - SCS = 30 kHz
  - f_c = 3.5 GHz
  - v = 240 km/h

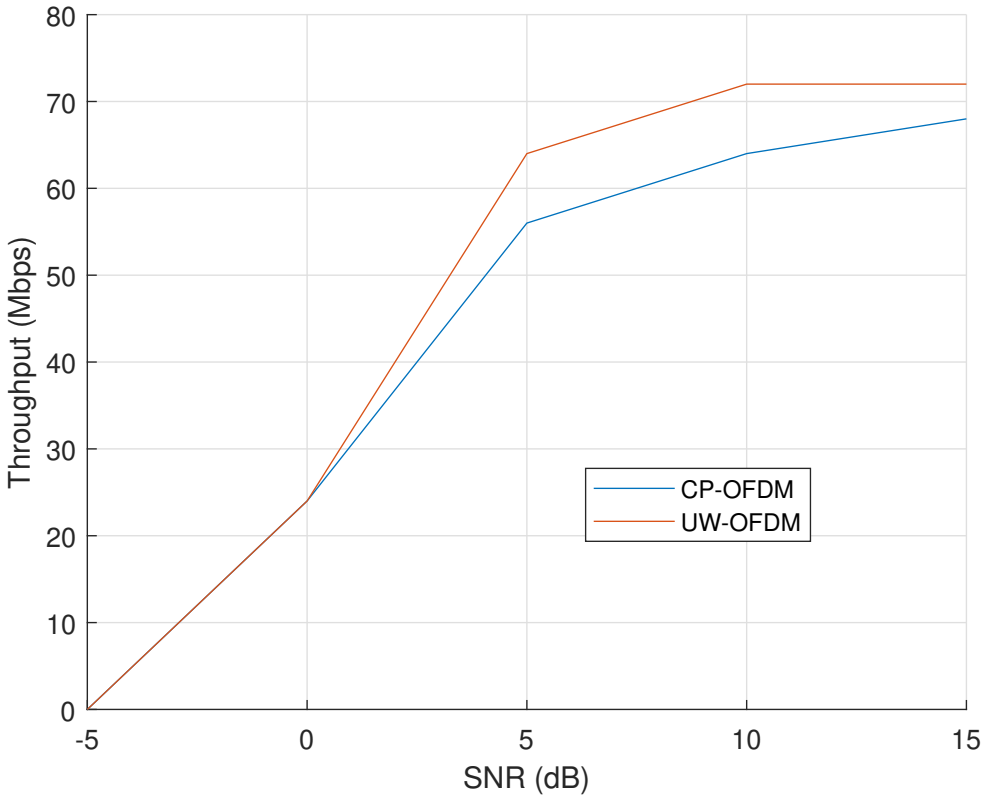

Figure 4.16. *Comparison of CP-OFDM and UW-OFDM in scenario 5*

- Scenario 6:
  - SCS = 15 kHz
  - f_c = 3.5 GHz
  - v = 160 km/h

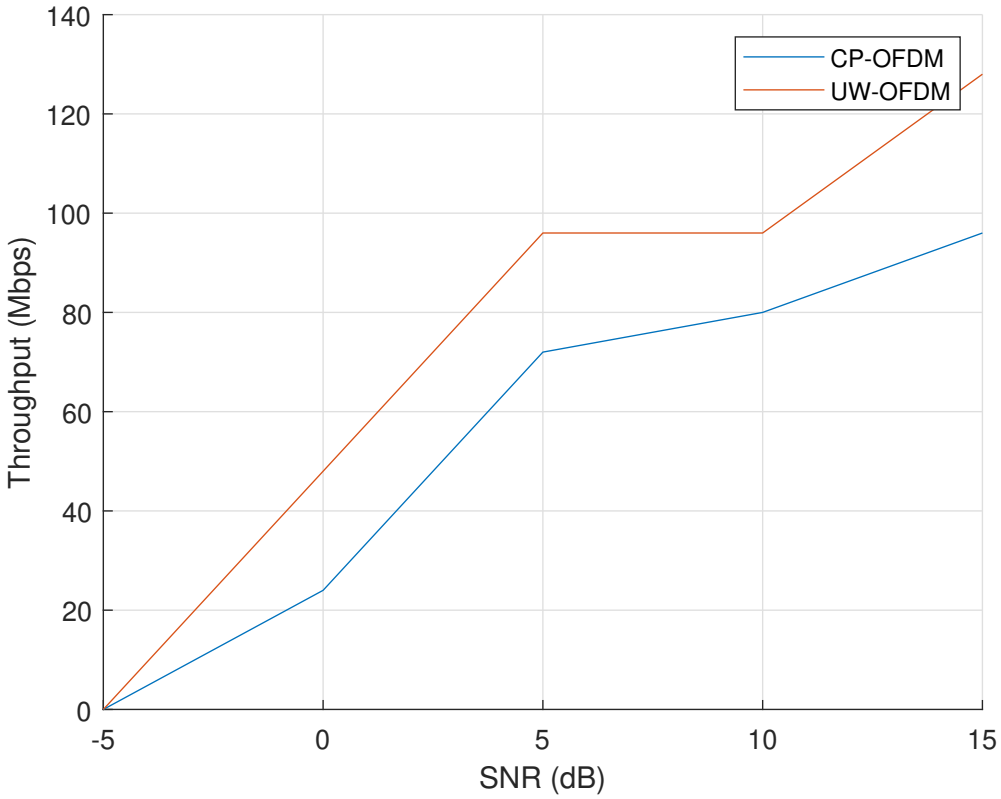

Figure 4.17. *Comparison of CP-OFDM and UW-OFDM in scenario 6*

- Scenario 7:
  - SCS = 15 kHz
  - f_c = 3.5 GHz
  - v = 240 km/h

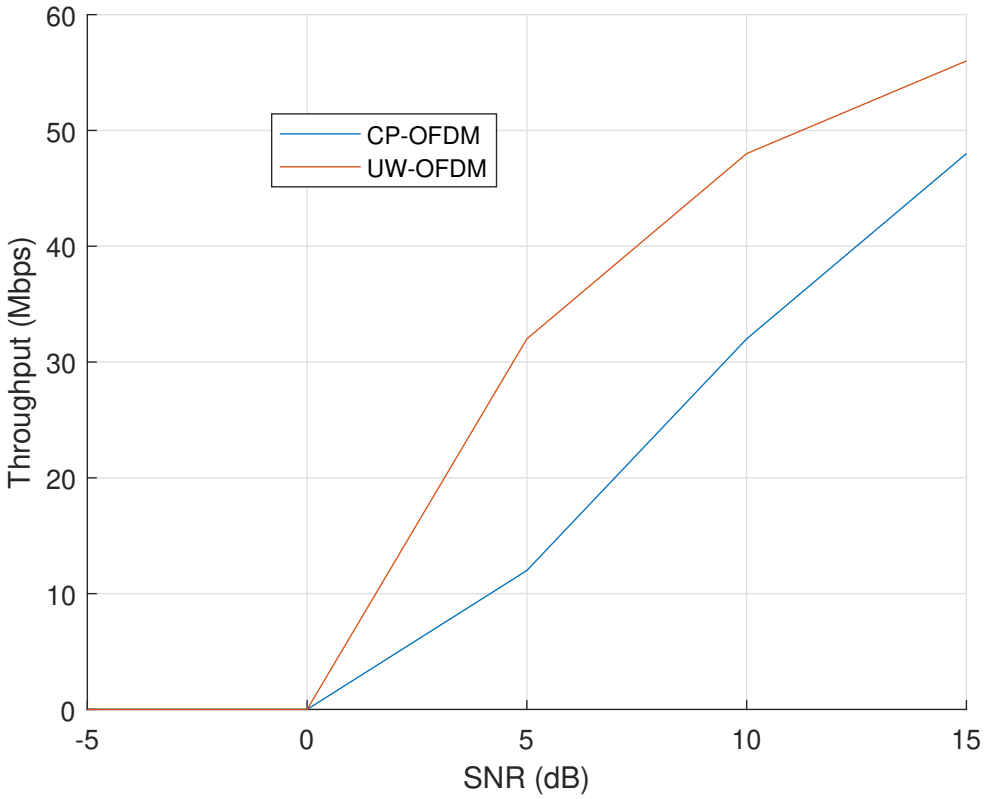

Figure 4.18. *Comparison of CP-OFDM and UW-OFDM in scenario 7*

- Scenario 8:
  - SCS = 60 kHz
  - f_c = 30 GHz
  - v = 160 km/h

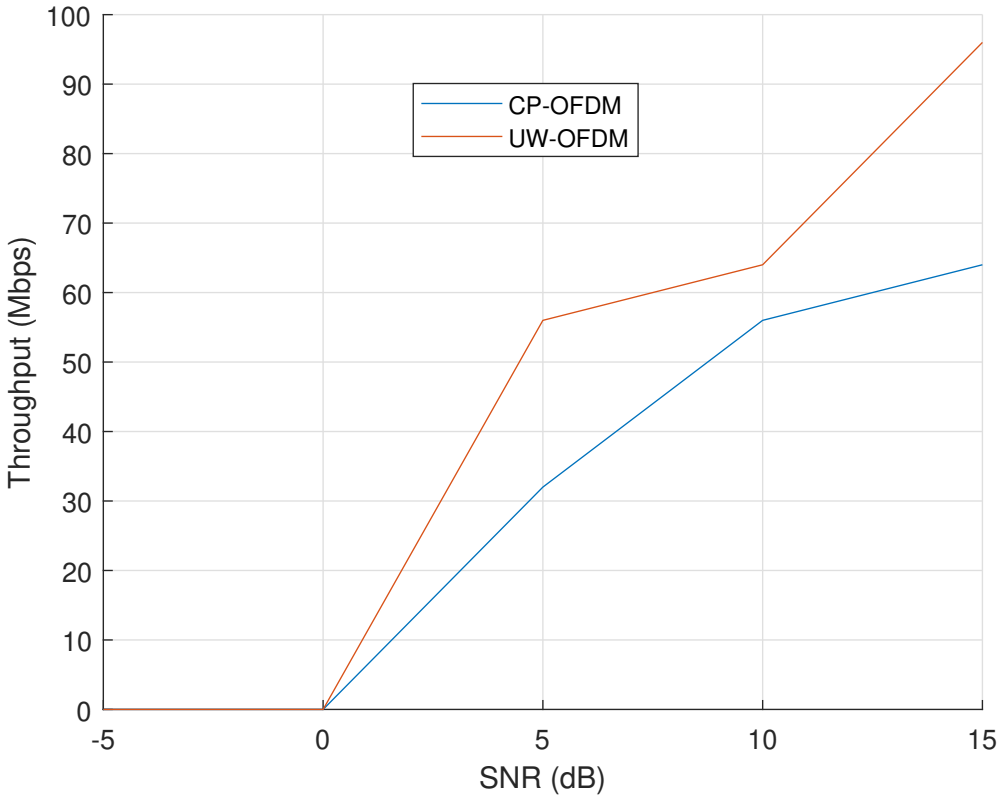

Figure 4.19. *Comparison of CP-OFDM and UW-OFDM in scenario 8*

- Scenario 9:
  - SCS = 60 kHz
  - f_c = 30 GHz
  - v = 240 km/h

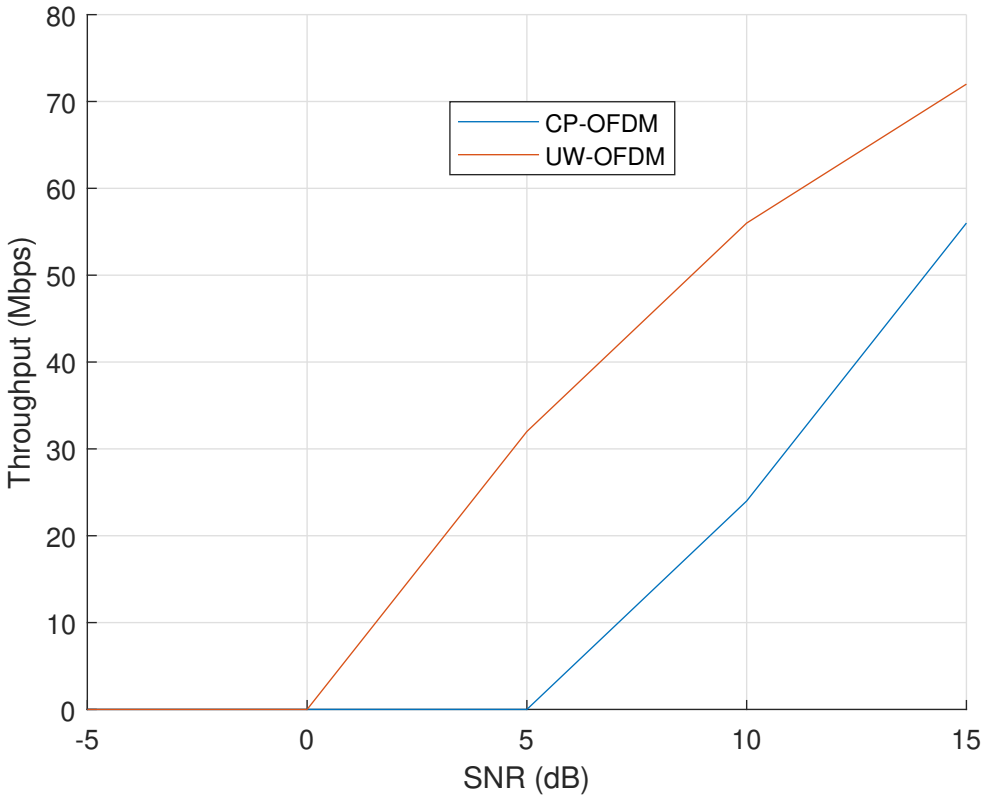

Figure 4.20. *Comparison of CP-OFDM and UW-OFDM in scenario 9*

The effect that the parameters have on the throughput is the same as in the CP-OFDM tests. As it is shown, when increasing either the carrier frequency or the device speed, the Doppler shift is increased, and therefore, the ICI increases, decreasing the final throughput. Also, when increasing the SCS, as the Doppler shift represents a smaller percentage of the total bandwidth of the subcarrier, the ICI is smaller than in the scenarios where the SCS is smaller. All these effects have been explained more in detail in the previous tests.

The only parameter that is not analyzed is the number of the DMRS symbols, as in the UW-OFDM scenarios they are not used for the channel estimation, as the coefficients of the channel are assumed to be known. So for every scenario analyzed, the channel coefficients are the ones obtained by the channel estimation in the CP-OFDM waveform for 4 DMRS symbols.

For all the simulations, the length of the UW was the same as the length of the CP, in order to make a fair comparison. Also, for the UW-OFDM simulations, a LMMSE estimator has been used, as it is the estimator that shows a better performance [3],[4],[5]. As it can be seen, the throughput offered by UW-OFDM is superior to the one offered by CP-OFDM in every scenario.

As the channel coefficients are assumed known for both waveforms, the different approaches for the channel estimation are not that relevant, and the main reason of having a higher throughput in UW-OFDM is the inclusion of the UW in the DFT period. In this way and as seen in figure 3.3, there is no need to use a guard interval, and therefore, the same number of frames is sent in a smaller period of time.

Therefore, in this thesis, the main reason of having a higher throughput in UW-OFDM is because the correct data received takes less time than in the CP-OFDM. In order to make a better comparison between both of them, the channel coefficients should not be assumed known and should be estimated by using the properties of UW-OFDM. However, the different studies this thesis is based on [3],[4],[5], do not have this approach.

5 CONCLUSIONS

The needs of the human being increase considerably and at an impressive speed, and therefore, new telecommunications technologies must meet these needs. As it has been shown, these needs vary and therefore require mobile networks that are capable of adapting to different situations that might require some coverage, speed, latency or mobility values.

In order to do so, it is necessary for the 5G technology to be able to adapt to these situations. As it has been shown, there are different parameters that have to be adjusted to suit each situation, and all of them affect in one way or another the total throughput obtained.

For the high speed scenarios, it has been shown that the speed and the carrier frequency are the main causes of the increase in the Doppler shift, which leads to a decrease in the throughput. In addition, it has also been shown that using a smaller number of DMRS symbols causes a worse channel estimation, since the interpolation has fewer points and therefore, the throughput also decreases. These parameters are not the only ones that affect the throughput, since it is also affected by the chosen numerology. A larger subcarrier spacing reduces the ICI, thereby increasing the number of correct detections in the receiver.

So it seems reasonable to look for configurations that include high SCS, such as 60 kHz, small carrier frequency, such as 3.5 GHz, and the maximum number of DMRS symbols, which is 4. By doing so, in this high speed scenarios, the throughput is going to be maximized.

Due to this variation and increase in people's needs, it is necessary to innovate by looking for other waveforms compatible with the requirements of future generations of mobile networks. Therefore, one of the alternatives proposed by the experts and, which has been analyzed in detail, is UW-OFDM. As we have seen, this waveform offers numerous advantages over CP-OFDM, such as higher spectral efficiency or better synchronization in the receiver. In addition, the obtained throughput has been slightly bigger compared to the one obtained with CP-OFDM.

However, this comparison is made using a channel whose coefficients of its impulse response are known, and therefore, it is not a realistic result. Finally, we can conclude that despite being an interesting alternative to the current 5G specifications, UW-OFDM has still a long way in front of it and it has to still be developed in order to be implemented

in future generations and obtain its full potential.

REFERENCES

[1] David Tse and Pramod Viswanath. *Fundamentals of Wireless Communication*. Cambridge University Press (2005).

[2] Gottapu Sasibhushana Rao. *Mobile Cellular Communication*. Andhra University College of Engineering, Departament of Electronic and Communication Engineering, 2013.

[3] Mario Huemer, Christian Hofbauer, and Johannes B. Huber. *Non-Systematic Complex Number RS Coded OFDM by Unique Word Prefix*. IEEE TRANSACTIONS ON SIGNAL PROCESSING, VOL. 60, NO. 1, JANUARY 2012.

[4] Mario Huemer, Christian Hofbauer, and Johannes B. Huber. *The Potential of Unique Words in OFDM*. Klagenfurt University, Institute of Networked and Embedded Systems, A-9020 Klagenfurt. University of Erlangen-Nuremberg, Institute for Information Transmission, D-91058 Erlangen , 2010.

[5] Mario Huemer, Alexander Onic, and Christian Hofbauer. *Classical and Bayesian Linear Data Estimators for Unique Word OFDM* . IEEE TRANSACTIONS ON SIGNAL PROCESSING, VOL. 59, NO. 12, DECEMBER 2011.

[6] ITU-R. Report M.2134 *Requirements related to technical performance for IMT-Advanced radio interface(s)* . 2008

[7] 3GPP TS 36.101 V16.3.0 *3rd Generation Partnership Project; Technical Specification Group Radio Access Network; Evolved Universal Terrestrial Radio Access (E-UTRA); User Equipment (UE) radio transmission and reception (Release 16)* . (2019-09).

[8] 3GPP TS 36.211 V15.6.0 *3rd Generation Partnership Project; Technical Specification Group Radio Access Network; Evolved Universal Terrestrial Radio Access (E-UTRA); Physical channels and modulation (Release 15)* . (2019-06).

[9] ShareTechNote, 5G Definition `http://www.sharetechnote.com/html/5G/5G_Definition.html`. Retrieved 23 October 2019

[10] 3GPP TS 38.101-1 V15.4.0 *3rd Generation Partnership Project; Technical Specification Group Radio Access Network; NR; User Equipment (UE) radio transmission and reception; Part 1: Range 1 Standalone (Release 15)* . (2018-12)

[11] 3GPP TS 38.211 V15.4.0 *3rd Generation Partnership Project; Technical Specification Group Radio Access Network; NR; Physical channels and modulation (Release 15)* . (2018-12)

[12] 3GPP TS 38.101-2 V16.0.0 *3rd Generation Partnership Project; Technical Specification Group Radio Access Network; NR; User Equipment (UE) radio transmission and reception; Part 2: Range 2 Standalone (Release 16)* . (2019-06)

[13] ShareTechNote, Resource grid in 5G NR `http://www.sharetechnote.com/html/5G/5G_ResourceGrid.html` Retrieved 23 October 2019

[14] 3GPP TS 38.202 V15.4.0 *3rd Generation Partnership Project; Technical Specification Group Radio Access Network; NR; Services provided by the physical layer (Release 15)* . (2018-12)

[15] ShareTechNote, DMRS symbols configuration for 5G NR `https://www.sharetechnote.com/html/5G/5G_PDSCH_DMRS.html`. Retrieved 23 October 2019

[16] 3GPP TS 36.104 V16.2.0 *3rd Generation Partnership Project; Technical Specification Group Radio Access Network; Evolved Universal Terrestrial Radio Access (E-UTRA); Base Station (BS) radio transmission and reception (Release 16)* . (2019-06).

[17] Ali A. Zaidi, Robert Baldemair, Hugo Tullberg, Håkan Björkegren, Lars Sundström, Jonas Medbo, Caner Kilinc and Icaro Da Silva. *Waveform and Numerology to Support 5G Services and Requirements*. Ericsson Research, Sweden. 2016

[18] Claudiu-Eugen Bota. *Implementación y simulacion de formas de onda para 4G*. Universidad Carlos III de Madrid, Departamento de Teoría de la Señal y Comunicaciones, 2017.

[19] Kun Chen Hu, Ana García Armada, and G. Pera. *Comparison of 5G candidate multicarrier waveforms in hardware testbed*. Universidad Carlos III de Madrid, Departamento de Teoría de la Señal y Comunicaciones, 2017.

[20] Michael Zoltowski. *Equations for the Raised Cosine and Square-Root Raised Cosine Shapes*. 2013

[21] D. Herbert. *Orthogonal Frequency Division Multiplexing*. 2003